12-2018

Identification of Sperm Chromatin Proteins as Candidate Markers of Stallion Fertility

Chelsea C. Ketchum
Utah State University

IDENTIFICATION OF SPERM CHROMATIN PROTEINS AS CANDIDATE MARKERS OF STALLION FERTILITY

by

Chelsea C. Ketchum

A thesis submitted in partial fulfillment
of the requirements for the degree

of

MASTER OF SCIENCE

in

Animal, Dairy, and Veterinary Sciences

Approved:

Ralph Meyer, Ph.D. Major Professor	Clay Isom, Ph.D. Committee Member
Kerry A. Rood, MS, DVM Committee Member	Laurens H. Smith, Ph.D. Interim Vice President for Research and Interim Dean of the School of Graduate Studies

UTAH STATE UNIVERSITY
Logan, Utah

2018

ABSTRACT

Identification of Sperm Chromatin Proteins as Candidate Markers of Stallion Fertility

by

Chelsea C. Ketchum, Master of Science

Utah State University, 2018

Major Professor: Ralph G. Meyer, Ph.D.
Department: Animal, Dairy and Veterinary Sciences

During spermatogenesis, histones are largely replaced by transition proteins and protamines in normal stallions. Incomplete nucleoprotein exchange results in the abnormal retention of histones and transition proteins, which is an indicator of poor sperm quality. Equine nucleoprotein exchange has not previously been investigated in detail, so that equine sperm chromatin quality problems, which are often responsible for poor breeding performance of stallions, are not well understood. In order to characterize chromatin remodeling events in stallion spermatogenesis and to identify proteins indicative of sperm chromatin defects, such as excessive amounts of histones, we identified antibodies that recognize equine testis-specific proteins of interest. Immunoblotting of testis and sperm protein lysates and immunofluorescence staining of histological tissue sections were used to identify candidate marker proteins of incomplete sperm chromatin maturation. Results of the study, which represents the first comprehensive characterization of the nucleoprotein exchange during spermatogenesis in

the stallion, challenge the paradigm that the main function of histone H4 lysine (hyper-) acetylation (concomitant H4K5 and H4K8 acetylation) is to facilitate nucleosome ejection during spermatid nuclear elongation to allow for transition protein and protamine insertion into the chromatin.

That paradigm was based on observations in mice and rats where H4 acetylation in several lysine residues occurs just prior to or during nuclear elongation. In contrast, the equine data presented here show strong acetylation of H4 in K5, K8 and K12 positions immediately after meiosis in round spermatids, independent of nuclear transition protein 1 deposition. Furthermore, results of H4K16 acetylation analyses underline the importance of this mark, which is likely mediated by DNA damage signaling pathways, emphasizing the importance of DNA repair processes for the exchange of nucleoprotein exchange in spermiogenesis and therefore, in extension, for male fertility. In addition, a revised description of the equine spermatogenic cycle is proposed here that is better aligned with human, mouse and rat spermatogenesis. Finally, the testis-specific histone variant TH2B was identified as a potential quantitative marker of equine sperm quality.

(71 pages)

PUBLIC ABSTRACT

Identification of Sperm Chromatin Proteins as Candidate Markers of Stallion Fertility

Chelsea C. Ketchum

During spermatogenesis, histones are largely replaced by transition proteins and protamines in normal stallions. Incomplete nucleoprotein exchange results in the abnormal retention of histones and transition proteins, which is an indicator of poor sperm quality. Equine nucleoprotein exchange has not previously been investigated in detail, so that equine sperm chromatin quality problems, which are often responsible for poor breeding performance of stallions, are not well understood. In order to characterize chromatin remodeling events in stallion spermatogenesis and to identify proteins indicative of sperm chromatin defects, such as excessive amounts of histones, we identified antibodies that recognize equine testis-specific proteins of interest. Immunoblotting of testis and sperm protein lysates and immunofluorescence staining of histological tissue sections were used to identify candidate marker proteins of incomplete sperm chromatin maturation. Results of the study, which represents the first comprehensive characterization of the nucleoprotein exchange during spermatogenesis in the stallion, challenge the paradigm that the main function of histone H4 lysine (hyper-) acetylation (concomitant H4K5 and H4K8 acetylation) is to facilitate nucleosome ejection during spermatid nuclear elongation to allow for transition protein and protamine insertion into the chromatin.

That paradigm was based on observations in mice and rats where H4 acetylation

in several lysine residues occurs just prior to or during nuclear elongation. In contrast, the equine data presented here show strong acetylation of H4 in K5, K8 and K12 positions immediately after meiosis in round spermatids, independent of nuclear transition protein 1 deposition. Furthermore, results of H4K16 acetylation analyses underline the importance of this mark, which is likely mediated by DNA damage signaling pathways, emphasizing the importance of DNA repair processes for the exchange of nucleoprotein exchange in spermiogenesis and therefore, in extension, for male fertility. In addition, a revised description of the equine spermatogenic cycle is proposed here that is better aligned with human, mouse and rat spermatogenesis. Finally, the testis-specific histone variant TH2B was identified as a potential quantitative marker of equine sperm quality.

ACKNOWLEDGMENTS

I would like to express my deepest gratitude to my major advisor, Dr. Ralph Meyer, and Dr. Mirella Meyer-Ficca who also acted as an advisor for their guidance and mentorship throughout my graduate studies. I would also like to thank my committee members, Dr. Kerry Rood and Dr. Clay Isom, and our lab managers Alexis McNeal and Miles Wandersee.

This work would not have been possible without support from the Animal, Dairy, and Veterinary Sciences department and Paul Loomis from Select Breeders Service for donating stallion semen samples, as well as funding from Utah Agricultural Experiment Station grant UTA01166.

I give special thanks to my boyfriend Gunter, who relocated to Utah with me and gave me unconditional patience and encouragement during this entire process. He supported and stood by me thru all the late nights and weekends preparing for exams, papers, and my thesis defense. In addition, I would like to express my appreciation to my mother, Laura, who gave me support and encouragement throughout my time at Utah State.

Chelsea C. Ketchum

CONTENTS

LIST OF TABLES

LIST OF FIGURES

Figure Page

CHAPTER I

INTRODUCTION

This study set out to characterize the timing of key events that happen during histone-to-protamine nucleoprotein exchange in spermatogenesis and to identify sperm chromatin proteins, such as excessively retained histones, as candidate markers for poor stallion fertility. Chromatin, which is loosely defined as the functional complex of DNA with DNA binding proteins and RNA, is important for the packaging of DNA into a compact, dense form. The sperm nucleus has a particularly dense form of chromatin to protect the paternal genetic material during transit to the egg.

During breeding soundness exams in horses, a semen analysis is performed on stallions to check for sperm numbers, sperm motility, and the percentage of morphologically normal sperm to determine gross reproductive abnormalities. Stallions that receive a normal breeding soundness exam may still contain subfertile semen as a result of genetic, environmental and management factors. Casey, Gravance, Davis, Chabot, and Liu (1997), found evidence that subfertile stallions produce sperm with significantly larger heads when compared to fertile stallions. This study proposes that these infertile sperm have less nuclear compaction than normal sperm and confirms that achieving a tightly packaged sperm chromatin structure is important for fertility. Sperm chromatin is very different from that of somatic cells (Braun, 2001; Rousseaux et al., 2004). In the archetypal mammalian, nongermline (somatic) cell, chromatin consists of nucleosomes complexed with superspiralized DNA, whereas sperm chromatin is extremely compact and based on protamine-DNA complexes. The compaction

("condensation") of chromatin is accomplished by a tightly regulated transition from the nucleosomal to a highly condensed chromatin structure that involves several remodeling steps in elongating spermatids (haploid male germ cells) during the postmeiotic phase of spermatogenesis, termed spermiogenesis. Replacement of most histones by transition proteins TP1 and TP2, and then later by protamines, changes the DNA structure from a supercoiled nucleosomal form to a relaxed toroid conformation (Grimes, Meistrich, Platz, & Hnilica, 1977; Kimmins & Sassone-Corsi, 2005; Zhao et al., 2004). The dramatic transition in DNA topology during nucleoprotein exchange requires controlled transient DNA double strand breaks (Marcon & Boissonneault, 2004; McPherson & Longo, 1992, 1993; Meyer-Ficca, Scherthan, Burkle, & Meyer, 2005; Risley, Einheber, & Bumcrot, 1986). These DNA strand breaks are mediated by topoisomerase 2 beta (TOP2B; McPherson & Longo, 1993; Morse-Gaudio & Risley, 1994; Roca & Mezquita, 1989) and their formation triggers activation of DNA damage signaling pathways, including those mediated by poly(ADP-ribosyl)ation and by ATM (ataxia telangiectasia mutated) serine/threonine kinase signaling (Ahmed, de Boer, Philippens, Kal, & de Rooij, 2010; Hamer et al., 2003; Leduc, Maquennehan, Nkoma, & Boissonneault, 2008; Meyer-Ficca, Lonchar, et al., 2011). We reviewed the currently available evidence for DNA damage-dependent chromatin remodeling in spermatids in Meyer, Ketchum, and Meyer-Ficca (2017). How the necessary DNA relaxation and the nucleoprotein transition from the nucleosomal to the protamine-based chromatin structure may be coordinated is not well understood, but it has been recognized that completion of spermatid chromatin maturation is important for male fertility in several species (de Oliveira et al., 2013;

Rathke, Baarends, Awe, & Renkawitz-Pohl, 2014). Not all histones are removed from the developing spermatid nucleus and the recent finding that the few histones that remain in human and mouse sperm are associated with promoters of specific genes and other genomic regions important for embryonic development suggests that retained histones may epigenetically regulate gene expression in the early embryo, and has renewed interest in the idea that sperm histones may have an important role in regulating gene expression in the early embryo (Arpanahi et al., 2009; Brykczynska et al., 2010; Carone et al., 2014; Erkek et al., 2013; Hammoud et al., 2011; Ihara et al., 2014; Schagdarsurengin, Paradowska, & Steger, 2012). In addition, the tight protamine-based sperm chromatin provides a resilient transport form of the paternal chromosome complement needed for the maintenance of genetic integrity between generations. Development of the final sperm chromatin structure requires multiple chromatin remodeling steps during spermatogenesis that involve a large number of specialized, in part testis-specific proteins, including non-canonical histone variants, and enzymes that impart posttranslational modifications on histones (Bao & Bedford, 2016).

Like in humans, cattle and other species, achieving a highly condensed sperm chromatin structure should also be important for stallion fertility and low chromatin quality should contribute to idiopathic infertility in the horse due to structural and epigenetic sperm nuclear defects. The diverse roles of noncanonical histone variants and histone modifications in chromatin remodeling processes during spermatogenesis have been recognized in mice and humans, but very little is known about them in the stallion. In order to evaluate potential causes of chromatin-based idiopathic infertility in stallions

as an emerging animal model, we therefore studied hallmark events of nucleoprotein transition in equine spermatogenesis using immunofluorescence staining of histological sections with the goal of understanding similarities and potential differences in chromatin remodeling events during spermatogenesis in mice and horses. To make comparisons more tractable, we reviewed the classic stallion spermatogenic cycle definition, and propose a revised system of simple tubule developmental stage identification that is more comparable to the well-accepted mouse and human stage models. Using predominant histological features we identified eight tubular cell association groups and arranged them to follow a similar developmental description as the mouse and human models (see Figure 7, shown and discussed later in Chapter II).

To this end, timing and cell type-specific protein expression of TH2B (histone cluster 1 H2B family member a, also known as testis-specific histone H2B and HIST1H2BA), TP1 (transition protein 1), PRM1 (protamine 1), and H2AFZ (also known as H2AZ and H2A histone family member Z) during spermatogenesis was investigated in this study. Because of their known implication with DNA relaxation and histone removal, the timing of H2AFX phosphorylation (H2A histone family member X, also known as H2AX and in its phosphorylated form as gamma-H2AX, here designated pH2AFX) was analyzed for the detection of DNA double strand break signaling, as well as histone H4 lysine acetylation events (H4K5ac, H4K8ac, H4K12ac and H4K16ac), were characterized in equine spermatogenesis and compared to corresponding events in the mouse, with unexpected results.

We also discovered that TH2B is a potential marker protein of poor sperm

chromatin quality that is retained in sperm in all horse semen samples we analyzed but TH2B levels differ several-fold between individual stallions. We are currently investigating to what extent sperm TH2B levels are correlated with stallion fertility.

CHAPTER II

REVIEW OF LITERATURE

Stallion Reproductive Anatomy and Physiology

The Testis

Horse testes are ovoid in shape and on average 8-12 cm long, 6-7 cm high and 5 cm wide (The Stallion: Breeding Soundness Examination & Reproductive Anatomy, 2007). The general anatomy of a testicle is shown in Figure 1. Seminiferous tubules populate the majority of the testis and are where spermatogenesis occurs. The seminiferous tubules are encased by connective tissue called the tunica albuginea and are reinforced by extensions of the tunica albuginea called septae (Reece, 2009). Sperm from the seminiferous tubules feed into the rete testis where they are then deposited into the efferent ducts and then into the head (caput) of the epididymis. The epididymis is used for storage of sperm and by passing through the ducts of the epididymis the sperm reach full maturity and become motile. The epididymis is divided into 3 parts: head (caput) of the epididymis, body (corpus) of the epididymis, and tail (cauda) of the epididymis. The majority of sperm storage occurs in the cauda of the epididymis. Sperm in the cauda epididymis will then flow into the ductus (vas) deferens to the pelvic urethra (Reece, 2009).

The Sperm

Individual equine sperm cells consist of three main segments: the head, mid-piece, and tail (Figure 2). The head encloses the nucleus, which contains the tightly

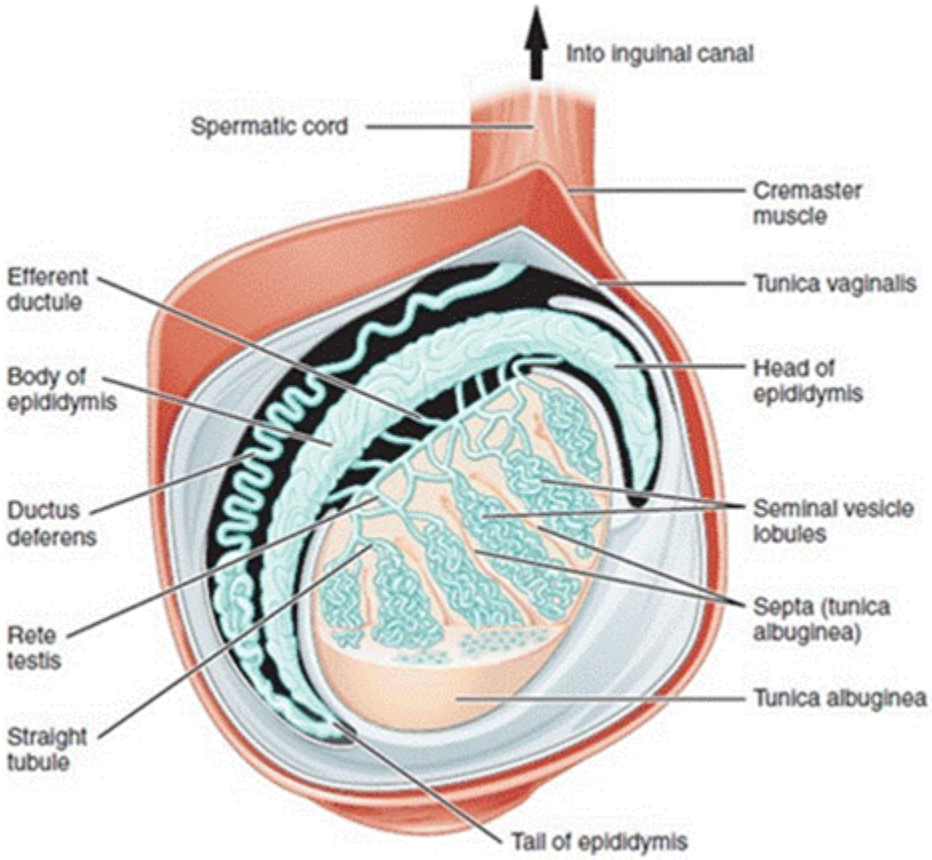

Figure 1. Anatomy of a testis. Seminiferous tubules occupy the largest area of the testes. Once sperm leave the tubules, they are stored in the epididymis. (Wikipedia)

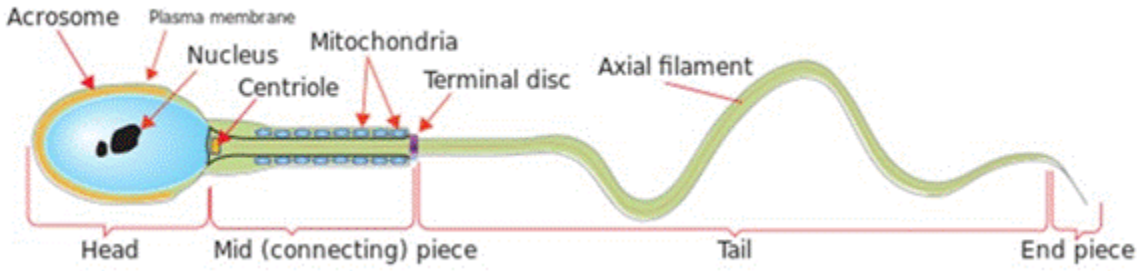

Figure 2. Anatomy of sperm. The head of the sperm contains the nucleus where the chromatin is stored. (Wikipedia)

condensed sperm chromatin. A cap-like structure called the acrosome covers the anterior half of the head and is used to penetrate the outer membrane (zona pellucida) of the mare's ovum. The mid-piece contains a central filamentous core that is surrounded by mitochondria. The mitochondria are arranged in a double spiral around these dense fibers throughout the length of the mid-piece. Roughly 60 spirals of mitochondria are found in the sperm of equids (Brito, 2007). The purpose of sperm mitochondria is to produce energy for motility. The tail is used to move and propel the sperm.

The average length of an equine spermatozoon is 60 μm (Pesch & Bergmann, 2006) and the average size of an equine sperm head is 5.33-6.62 μm long and 2.79-3.26 μm wide (Brito, 2007). Larger sperm head size is seen more frequently in subfertile stallions compared to fertile stallions (Casey et al., 1997). This correlation can be due in part to disturbances during chromatin condensation resulting in an insufficiently packed chromatin structure.

Spermatogenesis and the Spermatogenic Wave

Spermatogenesis, proliferation of spermatogonial stem cells and their development into spermatozoa, is a continuous process that occurs in cyclic pulses that "migrate" along the length of the seminiferous tubule (Johnson, Hardy, & Martin, 1990; Figure 3). In stallions, and other mammals such as mouse and human, a cross section of a seminiferous tubule embodies a predictable "association group" of certain spermatogenic cell types, depending on the phase of spermatogenesis that happens to occur in that tubule section. These association groups ("stages" of a tubule section) are species-specific and

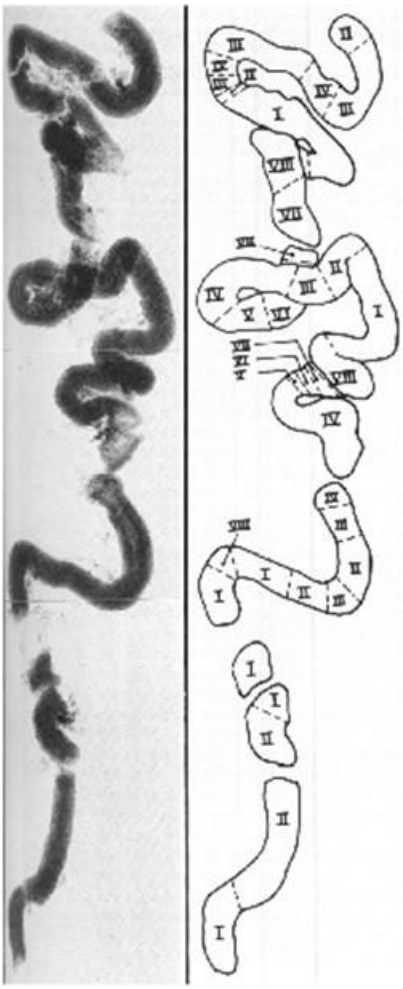

Figure 3. An equine seminiferous tubule segment shows the stages of the spermatogenic cycle. Stages are usually observed in consecutive order, however reversal of the order can occur (Johnson et al., 1990).

can be used to characterize the cycle of the seminiferous epithelium. Therefore, spermatids, which are the postmeiotic haploid cells, during a point in development, or stage, will always be associated with the same types of spermatogonia and spermatocytes (Clermont, 1963, 1972). These spermatogenic cell types consist of: A-spermatogonia, B-spermatogonia, spermatocytes (in meiotic prophase: preleptotene, leptotene, zygotene, pachytene and diplotene spermatocytes, as well as secondary spermatocytes undergoing

reduction cell division), spermatids, and spermatozoa. There are at least two types of A-spermatogonia, type A (dark) and type A (pale) (Clermont, 1972). Dark type A are reserve spermatogonial stem cells, while pale type A are spermatogonial stem cells that undergo mitosis and produce type B-spermatogonia. Type B-spermatogonia then divide to produce primary spermatocytes. Spermatocytes are the cells that undergo meiosis. Preleptotene, leptotene, zygotene, pachytene, and diplotene spermatocytes are all phases of prophase I during meiosis and are descriptively named according to the physical appearance of their chromosomes (Clermont, 1972). The first phase of prophase I is characterized by leptotene cells, in which chromosomes are now visually separate strands in the nucleus. The next phase is characterized by zygotene cells, in which one can see the homologous chromosome pairs line up together. As the nuclear volume grows, the chromosomes become thicker and shorten before entering the third phase, pachytene. This third phase of prophase I is where homologous recombination occurs. Succeeding the pachytene phase is the diplotene phase where chromosomes slightly split (Clermont, 1972). Following the diplotene phase, each spermatocyte will go through the two subsequent steps of cell division of meiosis resulting in 4 haploid daughter cells termed spermatids (Clermont, 1972).

The duration of the seminiferous epithelium cycle differs among mammals, as does the number of stages or cell association groups that are used to describe it. The classic view of the equine seminiferous epithelium cycle contains eight stages based on germ cell nuclear shape, bundle formation, luminal alignment, presence of cell types, and the release of spermatids (Johnson et al., 1990; Swierstra, Gebauer, & Pickett, 1974).

Swierstra et al. was able to map out the duration of the eight stages in stallion seminiferous epithelium using the injection of [^{3}H]-labeled thymidine and compare the results with other mammalian models. They found that the frequency of each stage in the stallion differed from the frequencies of other animal models when using the same system to classify stages. That study supports the claim that relative frequencies of the seminiferous epithelium stages are species-specific, but also that within a species it is rather constant (Swierstra et al., 1974). The total duration of spermatogenesis in the stallion is approximately 4.5 seminiferous epithelium cycles of ~12.2 days/cycle or 55 days total (Amann, 1981).

Previous Equine Spermatogenesis Model

The classic seminiferous tubule staging model used for stallions contains eight stages based on association groups of spermatogenic cell types (Figure 3). This equine staging model was first created by Swierstra et al. (1974) and was based on the presence of meiotic division, shape of the spermatid nuclei and the location of elongated spermatids. These eight stages were later reviewed and validated by others (Amann, 1981b; Johnson et al., 1990).

Figure 4 shows one cycle of stallion spermatogenesis; each column should be read upward from the spermatogenic cell types bordering the basement membrane to the cells close to the lumen (Cavalcanti et al., 2009). In stage I, round spermatids are the most advanced cell type present. Pachytene spermatocytes, leptotene spermatocytes, and A spermatogonia are also present during stage I. Stage II contains slightly elongated spermatids, pachtyene cells, leptotene cells, and A spermatogonia. Spermatids in stage III

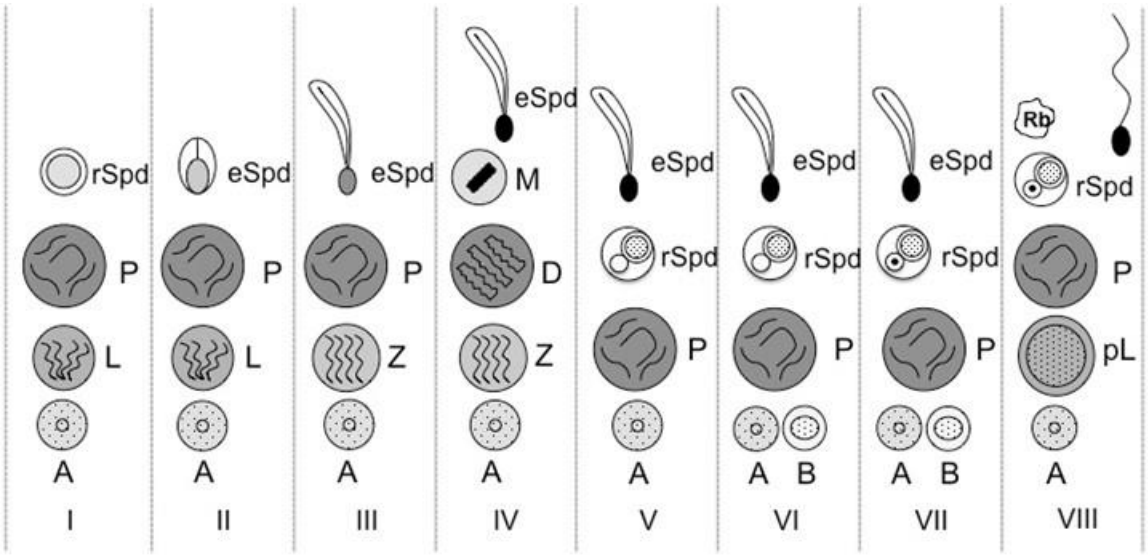

Figure 4. Classic equine stage identification model. This model begins with round spermatids (I) and progresses to elongating spermatids, meiosis, and ends with spermiation in stage VIII. (rSpd round spermatid; eSpd elongating spermatid; P pachytene; Rb residual bodies; pL preleptotene; L leptotene; Z zygotene; M meiotic plate, A A-spermatogonia, B B-spermatogonia). (Cavalcanti et al., 2009).

are more elongated and appear in clusters or bundles. Stage III contains pachytene cells, zygotene cells and A spermatogonia. In stage IV, the elongated spermatids begin to condense and secondary spermatocytes, zygotene cells and metaphase plates are present. A second generation of (round) spermatids is now present in stages IV through VIII. In stage V, elongated spermatids and secondary spermatocytes (spermatocytes after the first meiotic division) are present, as well as pachytene cells and A spermatogonia. The main difference between stage V and stage VI is the presence of A and B spermatogonia in stage VI. In stage VII, elongated spermatids continue to be present and begin to line up along the lumen. Round spermatids begin to develop their acrosome from the Golgi apparatus. Stage VII also contains pachytene cells, as well as A and B spermatogonia.

During stage VIII, fully elongated spermatids have begun to be released into the lumen and then into the epididymis (spermiation) and residual bodies are left in their place. Primary spermatocytes are present in both pachytene and preleptotene developmental steps. B spermatogonia divide during the previous stage, stage 7, and become preleptotene cells during stage 8. Additionally, A spermatogonia are present (Cavalcanti et al., 2009).

Revised Equine Spermatogenesis Model

Stallion spermatogenesis has not been used as a scientific model to the same extent human or mouse models are used. The classic equine stage map is set up opposite to the order of stages that is established with other commonly studied models, human and mice. To ensure a greater level of ease in the future when comparing stallion spermatogenesis with other species, a new staging model similar to those in human and mice is proposed.

Periodic acid-Schiff (PAS) staining was completed on stallion seminiferous tubules to evaluate whether an eight-stage model would be correct or a model with more stages, like in the mouse (12 stages) was needed. Stages one through eight were confirmed using this method (Figure 5, alongside the old stage classification in parenthesis). Stage I (V) in the new equine classiifcation model begins after the mitotic division and contains A spermatogonia, pachytene cells, as well as round and elongating spermatids. Stage II (VI) begins once B spermatogonia are present and the clusters of elongating spermatids start to migrate towards the lumen. Stage III (VII) begins once the clusters of elongated spermatids have started moving toward the lumen to when they

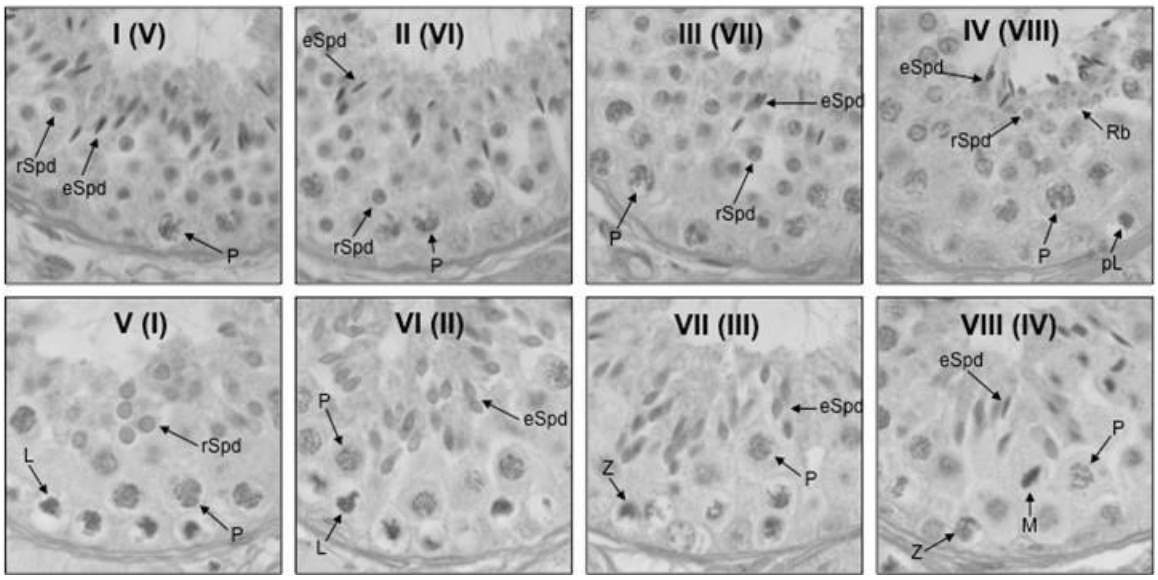

Figure 5. PAS staining showing the landmark cell types that are found during each stage. (rSpd round spermatid; eSpd elongating spermatid; P pachytene; Rb residual bodies; pL preleptotene; L leptotene; Z zygotene; M meiotic plate). The Roman numerals indicate the proposed, revised stage designations (the previous [classic] stage names are in parentheses; Ketchum, Larson, McNeil, Meyer-Ficca, & Meyer, 2018).

reach the lumen. Stage III (VII) also contains chromatin dots in the center of the round spermatids. Stage IV (VIII) begins once all the clusters of elongated spermatids reach the lumen and start to be expelled into the lumen. When elongated spermatids are expelled into the lumen during stage IV (VIII), residual bodies will be left in their place. Stage V (I) begins after all the elongated spermatids have left the lumen and only round spermatids are present. Stage VI (II) begins once the round spermatids start to elongate. Stage VII (III) occurs during spermatid elongation and contains zygotene cells. Stage VIII (IV) contains meiotic divisions and zygotene cells (Swierstra et al., 1974; Amann, 1981).

The new proposed equine spermatogenesis stage classification map shown in

Figure 6 confirms the basic observations of the previous equine spermatogenesis map, however moving around the order of these eight stages makes the new proposed model easier to compare with commonly studied models, mouse and human.

This proposed change to the current equine staging model appeared feasible and would be beneficial for future scientists looking to compare stallion spermatogenesis with more commonly used animal models, such as mouse and human. Currently, mouse and human seminiferous epithelium staging is set up where the cycle starts directly after meiotic division when secondary spermatocytes appear and progresses to mid-cycle

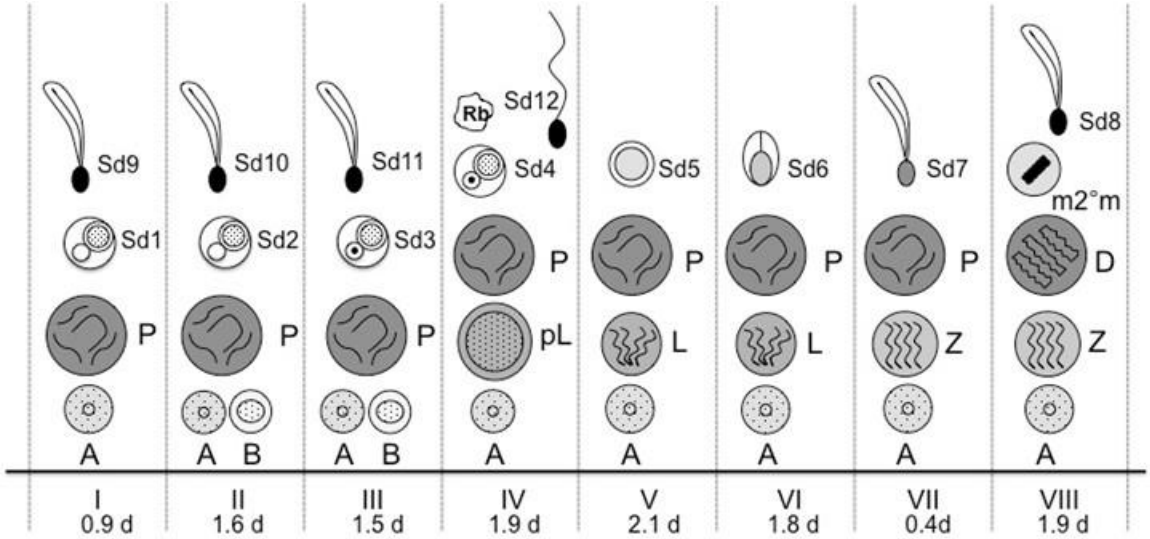

Figure 6. Proposed revised equine spermatogenesis map with stage intervals (days). The new classification model begins directly after meiotic divisions with secondary round spermatids during stage I and spermiation, i.e. the release of mature spermatids into the epididymis, leaving residual plasma bodies (Rb) behind, occurs during stage IV. The cycle ends with the meiotic division during stage VIII. This order of stages follows the murine spermatogenesis staging system, which has 12 stages (I-XII). In the new system, spermatids (Sd) are designated according to their developmental steps (Sd1-Sd12). Type A and B spermatogonia are located closest to the basal membrane (bottom). Spermatocytes are labeled according to their developmental stage in the meiotic prophase: P, pachytene; PL, preleptotene; Z, zygotene; L, leptotene; m2°m, secondary spermatocytes in meiotic division (Ketchum et al., 2018).

where spermiation occurs then progresses to the end of the cycle when meiotic division happens. The proposed equine staging model would mirror these landmark developments to create ease when comparing species (Figure 7).

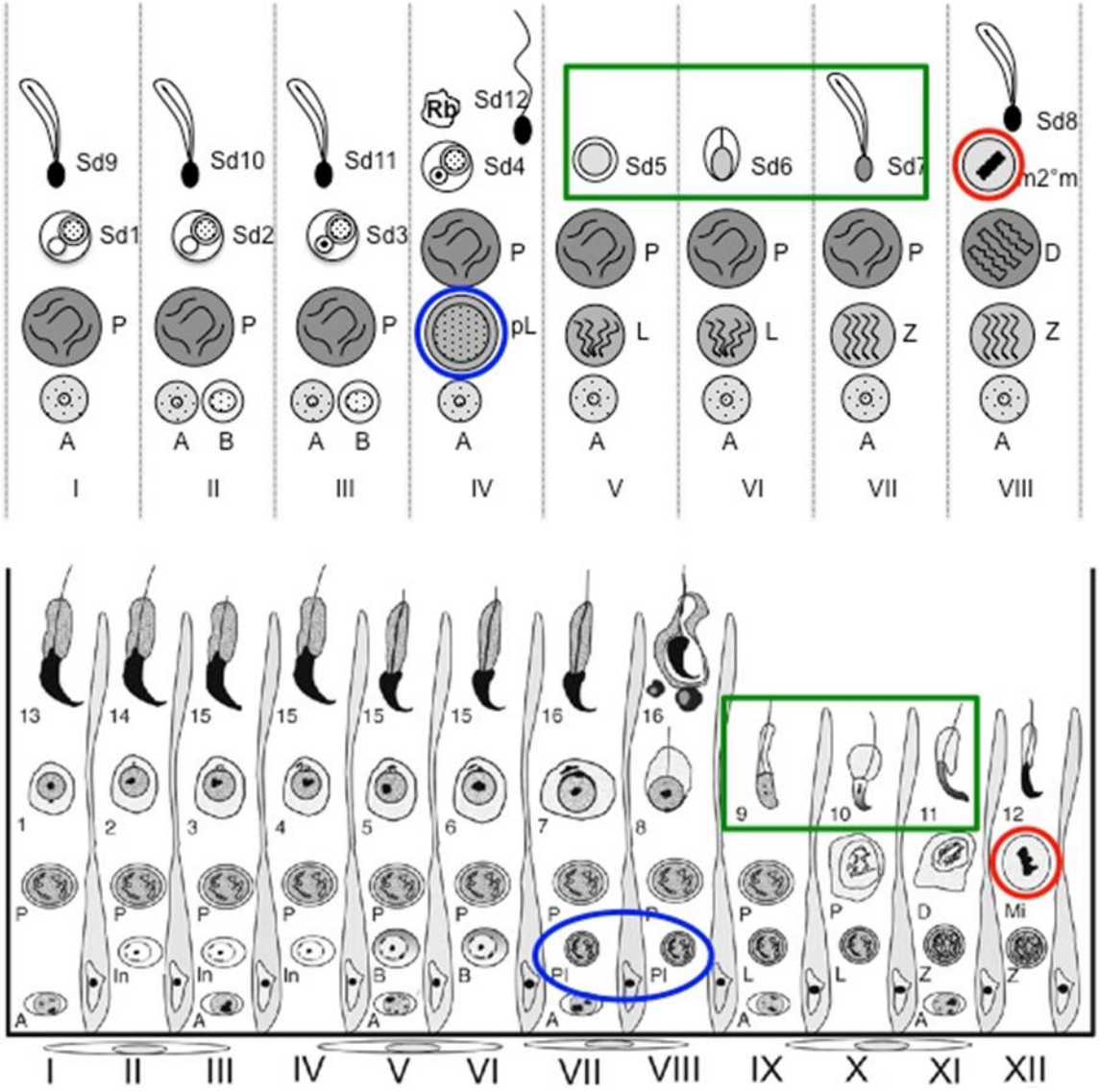

Figure 7. A comparison of new proposed equine staging model and the current mouse model showing landmark events during the seminiferous epithelium cycle. The horse model is on top and the mouse model is on bottom (Hess R. & Renato de Franca, L., 2008). Green box: spermatid nuclear elongation, red circle: meiotic division, blue circle: appearance of preleptotene spermatocyte concurrent with spermiation.

The classic view of the equine staging system is not as universally accepted as the one used in the mouse (Hess & Renato de Franca, 2008) and human (Clermont, 1966), where stage designations have been widely accepted in the scientific community. A recent study on equine spermatogonial stem cell markers used a new classification model that differs from the classic eight-stage model shown in Figure 4 (Costa et al., 2012). The group characterized the stages of the seminiferous epithelium using a system based on acrosome formation, morphology of developing spermatid nuclei and associations of the germ cells (Costa et al., 2012). Using this approach to stage identification, they came up with a 12-stage model that is similar in design to the mouse model. This 12-stage equine model is analogous to the mouse model, which also has 12 stages, and the cycle also begins with secondary spermatocytes directly after the meiotic division and ends with the meiotic division. The revised system by Costa et al. addresses the need to create an equine staging model more comparable to the mouse and human models. However, although this model is more comparable to mouse and human models, the equine seminiferous epithelium cycle cannot be easily divided into 12 stages. The reason is that stallion spermatogenesis does not appear to be as strictly synchronized as the mouse (12 stages) but it is more synchronized than human spermatogenesis (6 stages), resulting in fewer clearly recognizable association groups (8 stages as proposed here).

Chromatin Quality

In the eukaryotic cell, chromatin consists of a large variety of basic (positively charged) nucleoproteins that exist as a complex with DNA (negatively charged). The

smallest unit of chromatin is the nucleosome, which consists of DNA that is wrapped around an octamer of core histone dimers of H2A, H2B, H3, H4 and the linker histone H1 (Figure 8; Kornberg, 1974). In its simplest form this beads-on-a-string fiber of approximately 15 nm is superspiralized and H1 and other proteins can form a larger coil of inactive (not transcribed) chromatin, the 30 nm fiber. Higher chromatin orders into loops, coils and domains are formed by the binding of other chromatin binding proteins. Higher complex chromatin is constantly remodeled to allow accessibility to a multitude of protein factors involved in replication, transcription and repair of the DNA. The N-terminal domains ("tails") of core histones protrude from the nucleosome and are typically marked by post-translational modifications, such as acetylation, methylation or phosphorylation. The core histone proteins are also called "canonical" histones because they are encoded by gene clusters that are transcribed all at the same time, resulting in

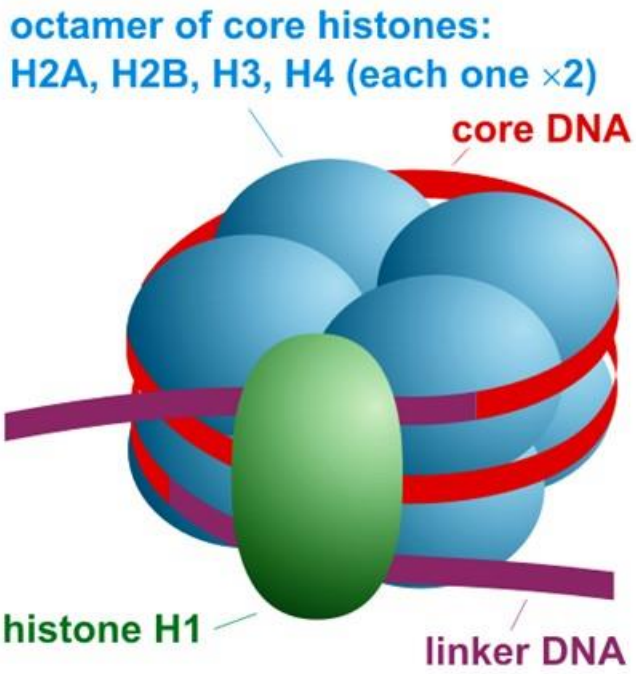

Figure 8. A nucleosome comprises an octamer of core histones (H2A, H2B, H3, and H4 and linker histone H1) that has DNA wrapped around it. (Wikipedia)

polycistronic RNA that is translated to give the individual 4 core histone proteins in equimolar quantities. There are also noncanonical histone variants that are encoded by individual genes scattered over the genome and that can be expressed in a tissue specific manner. Many of these histone variants and particularly several testis-specific histones are involved in chromatin regulation and transcription regulation during spermatogenesis (Montellier et al., 2013). Posttranslational modifications of canonical and non-canonical histones are currently subject to intense research because of their various structural and epigenetic functions. During spermatogenesis, histone variants including TH2A, TH2B, H2AX, H2AZ, MacroH2A, H3.3, H3t, and H1t appear to play important roles (Govin, Caron, Lestrat, Rousseaux, & Khochbin, 2004). In the testis, the acetylation of histone H4, the phosphorylation of H2AX, the presence of H2AZ in transcription start sites of genes, and insertion of testis-specific histones such as TH2B into the chromatin appear to have important, but not well-understood, roles during gene transcription, DNA damage signaling, and the exchange of histones for transition proteins and protamines during spermiogenesis (reviewed in Meyer et al, 2017). During spermatogenesis, core canonical histones are partly exchanged with histone variant counterparts by unknown mechanisms that may involve transcriptional gene activity (Maze, Noh, Soshnev, & Allis, 2014).

The majority of histone H2B is replaced with histone testis variant TH2B prior to its transition to protamines. The main alteration between canonical histone H2B and histone variant TH2B is in the N-terminal tail region, which may enable TH2B to destabilize nucleosomes and regulate gene activity. TH2B is important for normal spermatogenesis. When the genes for TH2A and TH2B are knocked out in the mouse,

males are sterile (Shinagawa et al., 2015). The absence of TH2B in these mutant mouse testes was countered by an overexpression of canonical histone H2B, but the absence of TH2A was not countered by an overexpression of canonical histone H2A.

In addition to TH2A, there are two main, nontestis specific histone variants that are expressed during spermatogenesis: H2AX and H2AZ. The phosphorylation of H2AX by the ATM/ATR kinase pathway is triggered by DNA double strand breaks and is essential for efficient DNA repair (Govin et al., 2004). During spermatogenesis DNA strand breaks occur endogenously to facilitate genetic recombination in spermatocytes and to allow relaxation of the DNA in elongating spermatids. When these controlled DNA double DNA strand breaks occur during spermatogenesis, prominent H2AX phosphorylation takes place. When H2AX was knocked out in mice, they became radiation-sensitive, immune-deficient, and infertile. Because phosphorylated H2AX (γH2AX) is needed for DNA repair, these mice had chromosomal instability and repair defects (Celeste et al., 2002). H2AZ has two isoforms, H2AZ.1 and H2AZ.2, that are encoded by independent genes and the resulting proteins differ by only three amino acids (Maze et al., 2014). Early embryonic death is associated with H2AZ.1 knockout in mice, which indicated that H2AZ.2 is not able to compensate for the removal of H2AZ.1 (Faast et al., 2001).

The acetylation of the N-terminal region of histone H4 reduces its positive charge and is believed to play a role in the removal of histones from the DNA and the insertion of transition proteins and protamines in their place. Acetylation of histone H4 occurs on four lysine residues, K5, K8, K12, and K16 (Zhang et al., 2002). These four acetylation

points can be present in various isoforms. Random acetylation can produce four mono-acetylated isoforms, six di-acetylated isoforms, four tri-acetylated isoforms, and one tetra-acetylated isoform that would include all four lysine residues to be acetylated. Each isoform may play a different role (Zhang et al., 2002). Elongating spermatids undergo genome-wide histone removal and the addition of transition proteins and subsequently protamines that will replace the majority of the histones (Wouters-Tyrou, Martinage, Chevaillier, & Sautiére, 1998).

In mice and humans, two transition proteins are expressed, transition protein 1 (TP1) and transition protein 2 (TP2). These proteins are only present during a short developmental time window when histones are being removed and protamines are being added. TP1 is a highly conserved protein across all mammals, while TP2 is only found in certain mammals, such as mouse and human (Bao & Bedford, 2016). When TP1 and TP2 were knocked out independently in mice, the two proteins would compensate for each other, while when both TP1 and TP2 were knocked out sperm saw a significant decrease in normal morphology, motility, and condensation of the chromatin.

Protamine also has two forms, protamine 1 (Prm1) and protamine 2 (Prm2). Horses and most other mammals only contain the Prm1 gene, while mice and human contain both Prm1 and Prm2 (Bao & Bedford, 2016). Unlike transition proteins, when either Prm1 or Prm2 gets knocked out, the mouse will become sterile (Cho et al., 2001). The normal process of histone replacement by protamines leaves only 3-5% and 10-15% of histones in place in mice and humans, respectively. It is not known what the exact percentage of retained sperm histones is in stallions. If more than the normal number of

histones are retained in sperm, infertility occurs with reduced implantation rates and elevated pregnancy loss but sperm maintain normal motility and fertilization capacity.

Excess histone retention in sperm can be detrimental to the fertility of the stallion and can cause low breeding cover rates. The foundation of this study was to identify chromatin proteins that can be detected in sperm, such as testis-specific histones, that will assist in identifying subfertile stallions. Stallion nucleoprotein exchange first needed to be investigated to locate suitable marker proteins present in sperm.

CHAPTER III

MATERIALS AND METHODS

Materials

A list of materials that were used during this research and what each material was used for is shown in Table 1. An antibody list is shown in Table 2, alongside where the antibodies were purchased, the type of antibody and the dilution factor for immunofluorescence and western blot assays.

Methods

Tissue Collection

Testis samples from three normal, mature stallions that were 3, 4, and 22 years of age, as well as from three immature, pubertal, yearling stallions were obtained as byproducts from routine castration procedures performed by veterinarians in a clinical setting, and immediately dissected into tissue samples of 1 cm^3 in size. These samples were quickly frozen in liquid nitrogen or on dry ice for biochemical analyses, or fixed in 10% formaldehyde or Bouin's solution for paraffin embedding and histological sectioning.

Mouse testes were obtained from wild-type 129SVE and BL6 mice that were housed, used and cared for as reviewed and approved by the Utah State University Institutional Animal Care and Use Committee (IACUC). In accordance with the current guidelines by the NIH Office of Laboratory Animal Welfare (OLAW), animals were

Table 1

List of Materials Used

Material name	Vendor	Cat. #	Uses
Acrylamide solution, 30%	Bio-Rad	161-0156	Western Blot
Ammonium persulfate (APS), 10%	Sigma-Aldrich	A3678-100G	Western Blot
β-mercaptoethanol	Sigma-Aldrich	M6250-100ML	Western Blot
Citric Acid, monohydrate	Sigma-Aldrich	C0706-500G	CMA3
CMA3 stock solution			CMA3
DAPI	Sigma-Aldrich	D8417-5MG	CMA3, Immunofluorescence
Donkey serum	Sigma	D9663-10ML	Immunofluorescence
Ethanol, 190 proof	Pharmco-Aaper	111000190	Immunofluorescence, PAS Staining
Glycine	VWR Life Science	0167-1KG	Western Blot
Hematoxylin solution	Sigma		PAS Staining
2x Laemmli buffer	Bio-Rad	161-0737	Western Blot
Methanol	Pharmco-Aaper		CMA3, Western Blot
$MgCl_2$	Sigma-Aldrich	M2670-500G	CMA3
Na_2HPO_4			CMA3
Nitrocellulose membrane			Western Blot
Odyssey blocking buffer			Western Blot
Periodic Acid solution	Electron Microscopy Science	26853-02	PAS Staining
Phosphate Buffered Saline tablets	Sigma-Aldrich	P-4417	Immunofluorescence, Western Blot
Ponceau S staining solution			Western Blot
RIPA buffer			Western Blot
Schiff's Reagent	Electron Microscopy Science	26853-01	PAS Staining
Sodium dodecyl sulfate (SDS)	Sigma-Aldrich	L4390-500G	Western Blot
Separating Gel Buffer (1.5 M Tris-HCl)			Western Blot
Stacking Gel Buffer (0.5 M Tris-HCl)			Western Blot
Target Unmasking fluid (TUF)			Immunofluorescence
TEMED	Sigma-Aldrich	T9281-50ML	Western Blot
Tris	VWR	97061-794	Western Blot
Tris Buffered Saline (TBS)			Western Blot
Tween 20	Sigma-Aldrich	P7949-500ML	Immunofluorescence
Vectashield			CMA3, Immunofluorescence
Xylene			Immunofluorescence, PAS Staining

Table 2

List of Antibodies Used for Immunofluorescence and Western Blot Analysis

Antibody name	Vendor	Type	Cat. #	Lot #	IF Dilution	WB Dilution	Research resource identifier (RRID)
Rabbit anti- TH2B	Upstate	Polyclonal	07-680	30338	1:200	1:2000	AB_417395
Mouse anti- γH2AX	Millipore	Monoclonal	05-636-I	2745891	1:150	1:2000	AB_309864
Rabbit anti- H2AZ (ChIP grade)	Abcam	Polyclonal	ab4174	30338	1:100	1:1000	AB_304345
Rabbit anti- TP1	Novus Biologicals	Polyclonal	NBp1-55356	QC22236-41495	1:200	1:2000	AB_11017259
Mouse anti- Prm1	Briar Patch	Monoclonal	HUP1N	N/A	1:100	N/A	AB_2651186
Rabbit anti- hyperacetylated H4	Millipore	Polyclonal	06-946	29860	1:200	1:1000	AB_310310
Rabbit anti- Histone H4 (acetyl K5) (ChIP grade)	Abcam	Monoclonal	ab51997	GR67153-12	1:300	1:10000	AB_2264109
Rabbit anti- Histone H4 (acetyl K8) (ChIP grade)	Abcam	Monoclonal	ab45166	GR53193-20	1:200	1:5000	AB_732937
Rabbit anti- Histone H4 (acetyl K12)	Abcam	Monoclonal	ab177793	GR208181-2	1:1000	1:10000	AB_2651187
Rabbit anti- Histone H4 (acetyl K16)	Abcam	Monoclonal	ab109463	GR59815-13	1:200	1:2000	AB_10858987
Mouse anti- Tubulin	Sigma	Monoclonal	T9026	115M4827V	N/A	1:5000	AB_477593
Donkey anti- Mouse CY3	Jackson ImmunoResearch	Polyclonal	715-165-150	124774	1:200	1:2000	AB_2340813
Donkey anti- Mouse Alexa Fluor 488	Jackson ImmunoResearch	Polyclonal	715-546-150	101010	1:200	1:2000	AB_2340849
Donkey anti- Rabbit CY3	Jackson ImmunoResearch	Polyclonal	711-165-152	100581	1:200	1:2000	AB_2307443
Donkey anti-Rabbit Alexa Fluor 488	Jackson ImmunoResearch	Polyclonal	711-546-152	100704	1:200	1:2000	AB_2340619

humanely euthanized for necropsy using carbon dioxide asphyxiation followed by cervical dislocation as recommended by the American Veterinary Medical Association (AVMA). Testes were either snap frozen or fixed in 10% formaldehyde similar to the horse testis samples, and further processed as described above for the equine tissue samples.

Sperm Collection and Preparation

Equine sperm samples were leftover material from artificial insemination procedures obtained as anonymized samples from different veterinary clinics and Select Breeding Service (Chesapeake City, MD). Raw semen samples were shipped either frozen or cooled and frozen upon arrival. Semen were thawed and stored on ice. One milliliter of raw semen combined with 9 ml of precooled PBS. It was then centrifuged for 5 minutes at 1000 x g and the supernatant was carefully removed. The pellet was suspended again in fresh precooled PBS. After resuspension, 10 mcl was removed and diluted with 90 mcl of PBS. Ten microliters of sample were then used for cell count using an improved Neubauer counting chamber (Fuchs-Rosenthal system). After counting, aliquots of each sample were made and spun down in a centrifuge for 2 min at 10,000 x g. The supernatant was carefully removed and the remaining sample was aliquotted and frozen at -80°C. One aliquot was resuspended in Laemmli buffer (98°C) for SDS polyacrylamide electrophoresis and subsequent immunoblot analyses. Sperm smears were generated on glass slides to confirm normal sperm morphology.

CMA3 Assay

Positive and negative control mouse sperm smear slides were used in addition to the stallion sperm smear slides to ensure the procedure worked. Sperm smear slides were fixed in methanol for 20 minutes at -20°C. Slides were then air-dried and incubated with 100µl of CMA3 working solution in the dark for 30 minutes at room temperature. When adding the CMA3 working solution, the start time was staggered to guarantee each slide was incubated for exactly 30 minutes. After the 30-minute incubation time, the slides were briefly dipped in Mcllvaine buffer and the excess liquid was removed. Slides were then mounted with 50µl of Vectashield/DAPI and a glass slide cover was added. Images were taken using a Zeiss Axioscope microscope at 63x magnification with oil immersion.

Periodic Acid-Schiff Staining

Testis tissue samples were taken from mature stallions and mice and were embedded in paraffin on slides for periodic acid-Schiff (PAS) staining. Testes slides were first dewaxed in vertical slide staining jars with 5-minute incubation periods with 100% xylene, 100% ethanol, 80% ethanol, 50% ethanol, and 20% ethanol then hydrated with deionized water. Slides were then immersed in Periodic Acid Solution for five minutes at room temperature. Slides were rinsed in several changes of distilled water then were immersed in Schiff's Reagent for 15 minutes at room temperature. Slides were washed in running tap water for 5 minutes then were counterstained using Hematoxylin solution for two minutes. Slides were rinsed in running tap water then dehydrated, cleared, and mounted using 15µl of xylene based mounting media. Testes slides were imaged using a Zeiss AxioVision epifluorescence microscope at 63x magnification.

Immunofluorescence

Testes tissue sections were dewaxed in vertical slide staining jars with five-minute incubation periods with 100% xylene, 100% ethanol, 80% ethanol, 50% ethanol, 20% ethanol, and 100% PBS buffer. Slides were incubated in hot antigen retrieval solution (~10% citrate buffer) for ten minutes, and then washed in PBS for five minutes. Slides were incubated in 100µl of 3% donkey serum in a humidity chamber for one hour. After blocking with the 3% donkey serum, slides were washed in PBS for five minutes. Slides were blocked using using 3% donkey serum in PBS prior to overnight incubation (4°C) with primary antibody. The next day, slides were washed in PBS three times for five minutes each and incubated with secondary antibody for 45 minutes at 37°C, which was either a donkey anti-mouse (1:200), or a donkey anti-rabbit antibody (1:200, both Jackson ImmunoResearch), which were either labeled with CY3 or Alexa Fluor 488 fluorescent dyes to detect each primary antibody. Slides were washed in PBS three times for ten minutes each and mounted with coverslips and anti-fade mounting medium (Vectashield) containing 1 µg/mL 4, 6-diamidino-2-phenylindole (DAPI) to stain nuclear DNA. Slides were also incubated with fluorescent labeled secondary antibodies in absence of primary antibodies in the experiments to control for secondary antibody unspecific binding and tissue autofluorescence. Images were taken using an epifluorescence microscope (Zeiss AX10 scope.A1) equipped with LED illumination (Xcite 120) and oil immersion objectives including a 63x magnification lens (Zeiss Plan Apochromat 63/1.4). A computer-controlled charge coupled device (CCD) black-and-white camera (Zeiss Axiocam) was used for microphotography of fluorescent images. In

order to create merged images of DAPI- and antibody-labeled structures, individual microphotographs were false-colored using Adobe Creative Cloud Photoshop (version 7.1) that were only processed by adjusting brightness and contrast. Overlays (merged images) were created using the "Exclusion" function of the software. Images were imported into Microsoft PowerPoint and cropped to size where appropriate. In PowerPoint, some images were adjusted for brightness and contrast as well. Criteria for positive labeling of a given cell type by a certain antibody were established as nuclear fluorescence visibly above background and not present in a secondary-antibody-only negative control and present in testis sections of at least two of the three mature stallions (not shown, see Ketchum et al., 2018). Stallion spermatogenesis stage identification from immunofluorescence was performed according to Johnson et al. (1990).

Western Blot

Testes and semen samples were separated on a 15% SDS-PAGE 1.5mm gel. The gel was then blotted onto a nitrocellulose membrane. The membrane was stained using Ponceau S and destained using PBS. The membrane was incubated in primary antibody solution overnight on a rocker at 4°C. Alpha-Tubulin was used as a control. The next day, the membranes were incubated on a rocker for 30 minutes at room temperature. Membranes were removed from sealed packs and washed in TBS/ 0.1% Tween20 for 5 minutes for three times. Appropriate secondary antibody solution was applied, and incubated in the dark at room temperature on a rocker for 30-60 minutes. The membranes were then washed in TBS/ 0.1% Tween20 for 10 minutes for 3 times. Images were then scanned using a fluorescence imaging and quantification system (Typhoon Scanner).

CHAPTER IV

RESULTS

Stallion Testes

Testis-Specific Histone H2B (TH2B)

To explore the potential of using testis-specific histone H2B (TH2B) as a chromatin marker we studied its expression pattern in stallion testis using immunofluorescence and its presence in immature and mature testis and sperm using western blot analysis. Based on previous work done by Johnson et al. (1990), eight stages of stallion spermatogenesis were observed for TH2B antibody detection in immunofluorescence. As shown in Figure 9, TH2B is detected in cells throughout meiotic prophase in meiosis and in round and elongating spermatids. During spermatid elongation in stages VI and VII, histones are being removed and transition proteins and protamines are being added. This event leads to the predominant eviction of TH2B from the nucleus and consequently a decrease of the fluorescence staining during stage VII in elongating spermatids. Throughout the later stages, stages VIII, I, II, III and IV, TH2B is present in the round spermatids and pachytene spermatocytes.

In order to validate the antibodies, Western blot analysis was completed using protein extracts prepared from mature and immature stallion testes. As shown in Figure 16, TH2B was detected at approximately 14 kDa in mature testis, confirming that a protein of the correct size was recognized by the antibody in a mature but much less in a prepubertal testis lysate. Normal stallions will naturally retain some of their histones, but

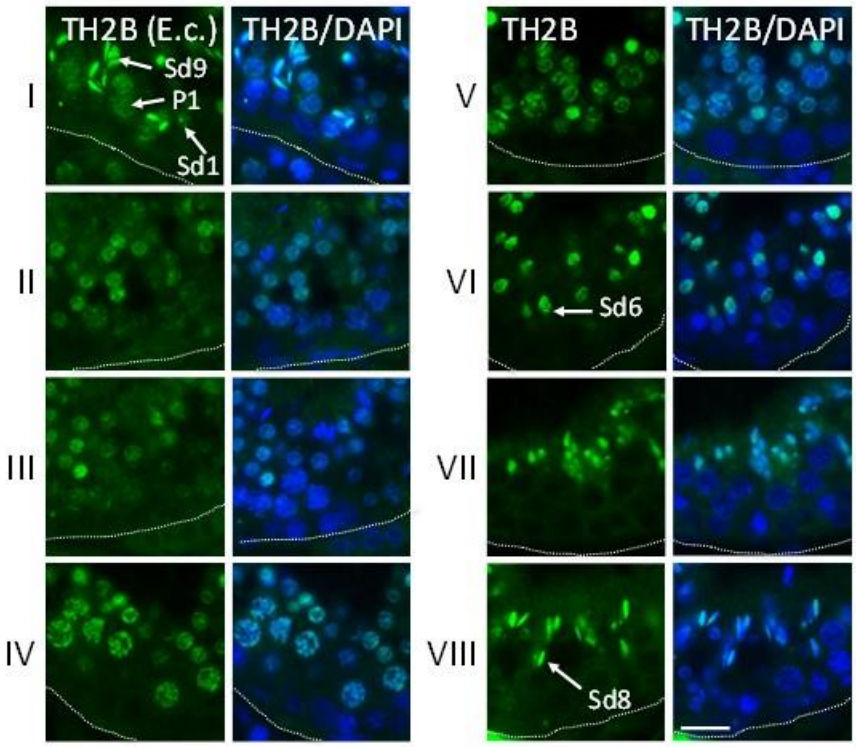

Figure 9. Immunofluorescence of testis-specific histone TH2B. The noncanonical histone variant TH2B was expressed in stallion pachytene spermatocytes and began to become undetectable as elongating spermatid chromatin condense (stages VIII-II, Sd8 –Sd10).

excess histone retention may be used as a marker for poor fertility. The two immature horse testes show a distinctly faint band compared with the mature testis, which was expected due to immature testis having not entirely complete spermatogenesis.

Acetylation of histone H4

To study the role of hyperacetylated H4 during histone eviction, we looked at its expression pattern in stallion testis using immunofluorescence and its presence in immature and mature testis and sperm using western blot analysis. As shown in Figure 10, hyperacetylated H4 is present in round spermatids during stage V and slightly elongating spermatids during stage VI. During stages VII and VIII, the presence of

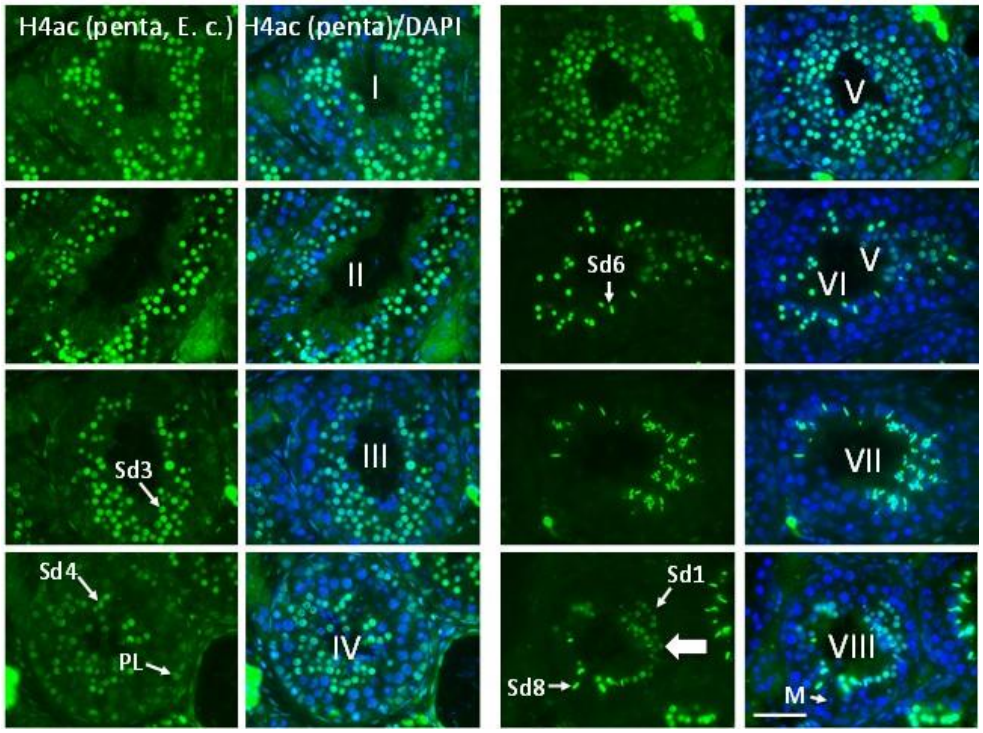

Figure 10. Immunofluorescence of hyperacetylated H4. Sd: spermatid steps, PL: preleptotene spermatocyte. Note that round Sd8 spermatids show H4 acetylation immediately after their formation through meiotic division in stage VIII (arrow).

hyperacetylated H4 slowly decreases and it is no longer present in elongated step 9 spermatids (Sd9) during stage I. Immediately after meiosis, hyperacetylated H4 is found in round spermatids and in preleptotene cells during stage IV. Importantly, this finding differs to the current paradigm that hyperacetylated H4 is only present in early elongating spermatids during the early stages and preleptotene cells, which was based on findings in mice, rats (Meistrich, Trostle-Weige, Lin, Bhatnagar, & Allis, 1992) and humans, which is thought to facilitate histone removal. Hyperacetylated H4 was also found in preleptotene spermatocytes, confirming findings in the mouse and in humans, and confirming validity of the antibody used in the present study.

To verify that the H4 hyperacetylation antibody truly recognizes the correct

target, we repeated the procedure with wild type mouse testis and confirmed the expression pattern results with the results found by Govin et al. (2004). The "hyperacetylation" recognized by the antibody refers to the acetylation of H4K5 and H4K8, but not K16, lysine residues. These H4K5 and H4K8 acetylation marks are of significance because they are recognized by the bromodomain protein BRDT, which has been implicated in the removal of nucleosomes from the DNA to allow for TP1 and protamine deposition. The unexpected result we found in equine, that H4K5 and H4K8 are acetylated a whole week prior to the histone-to-protamine exchange, raises the question to what extent H4 hyperacetylation, i.e. the acetylation of H4 in K5 and K8 position is the true signal for nucleosome eviction in elongating spermatids, which is the current understanding based on findings in mouse and human. To further exclude that the antibody we used gave incorrect results, separate antibodies recognizing H4K5ac, H4K8ac, H4K12ac and H4K16ac were used individually to corroborate our findings regarding the hyperacetylation of H4. These four main acetylation marks have been believed to make up hyperacetylation of histone H4 (Zhang et al., 2002). All antibodies used in the present study were also used in immunofluorescence and western blot analyses to compare their expression patterns with hyperacetylated H4 to validate the paradigm-shifting results.

H4K5ac was present in round spermatids from after meiosis in stage VIII through the mid-late, elongating spermatids of stages VI through VIII (Figure 11). H4K5ac was also present in preleptotene cells during stage IV. These results were similar to the results found for hyperacetylated H4.

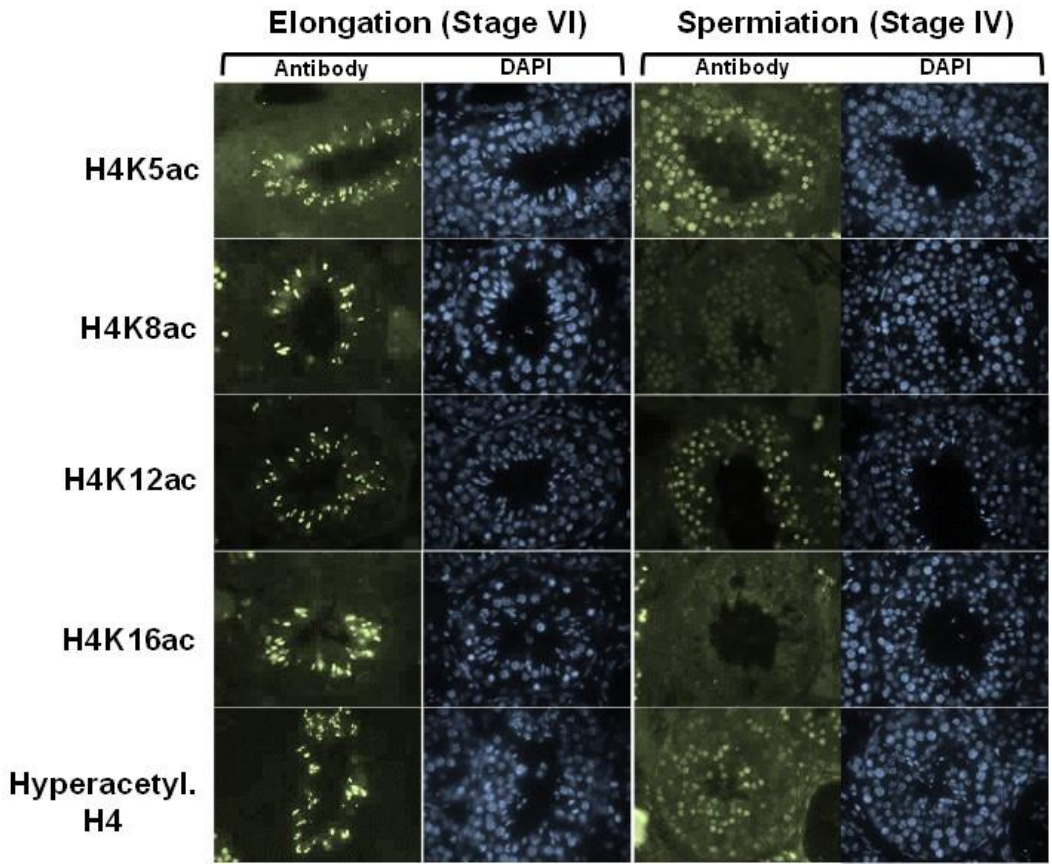

Figure 11. Immunofluorescence of H4K5ac, H4K8ac, H4K12ac, H4K16ac, and hyperacetylated H4 (H4ac penta) in the stallion. Spermatid elongation occurs during stage six and spermiation occurs during stage four.

Immunofluorescence analyses using H4K8ac antibodies gave exactly the same results as with the H4K5ac antibodies, staining the same cell types, which were again identical to the findings using the hyperacetylated H4 antibody (Figure 11).

H4K12ac was detected in all spermatids up to step Sd10 (Figure 11), and in addition in pachytene cells of all stages. Based on these data, H4K12 acetylation is an unrelated event to H4 hyperacetylation and not recognized by the "hyperacetylated H4" antibody.

H4K16ac was only expressed in elongating Sd6 spermatids during stage 6,

(Figure 11). These results are different to what was found in H4K5ac, H4K8ac, and hyperacetylated H4 in equine, but they are in line with the current paradigm that H4K16 acetylation only occurs during histone removal.

Western blot analysis was completed on immature and mature testes lysates using the antibodies for H4 hyperacetylation, H4K5ac, H4K8ac, H4K12ac and H4K16ac. As shown in Figure 16, hyperacetylated H4 was detected at approximately 11 kDa in both immature and mature testes. H4K5ac, H4K8ac, H4K12 and H4K16 were detected separately at approximately 11 kDa in immature and mature testes.

γH2AX and H2AZ

The expression pattern of the histone H2A variant H2AZ was studied using immunofluorescence and western blot, along with the phosphorylation of H2AX. As shown in Figure 12, γH2AX is expressed in elongating spermatids during stages VI through I. Gamma-H2AX is also present in leptotene cells during stages V and VI and in zygotene cells during stages VII, VIII, and I. XY bodies on pachytene cells during all stages have strong γH2AX staining.

As shown in Figure 13, H2AZ is expressed in round spermatids during stage 5 and in elongating spermatids during stages 6 through 8. H2AZ is present during all steps of prophase I during meiosis, leptotene cells, zygotene cells, pachytene cells, and diplotene cells. Expression of H2AZ is also found in secondary round spermatids during stages 1 through 4.

Western blot analysis was completed on immature and mature testes (Figure 16, shown later in this chapter).

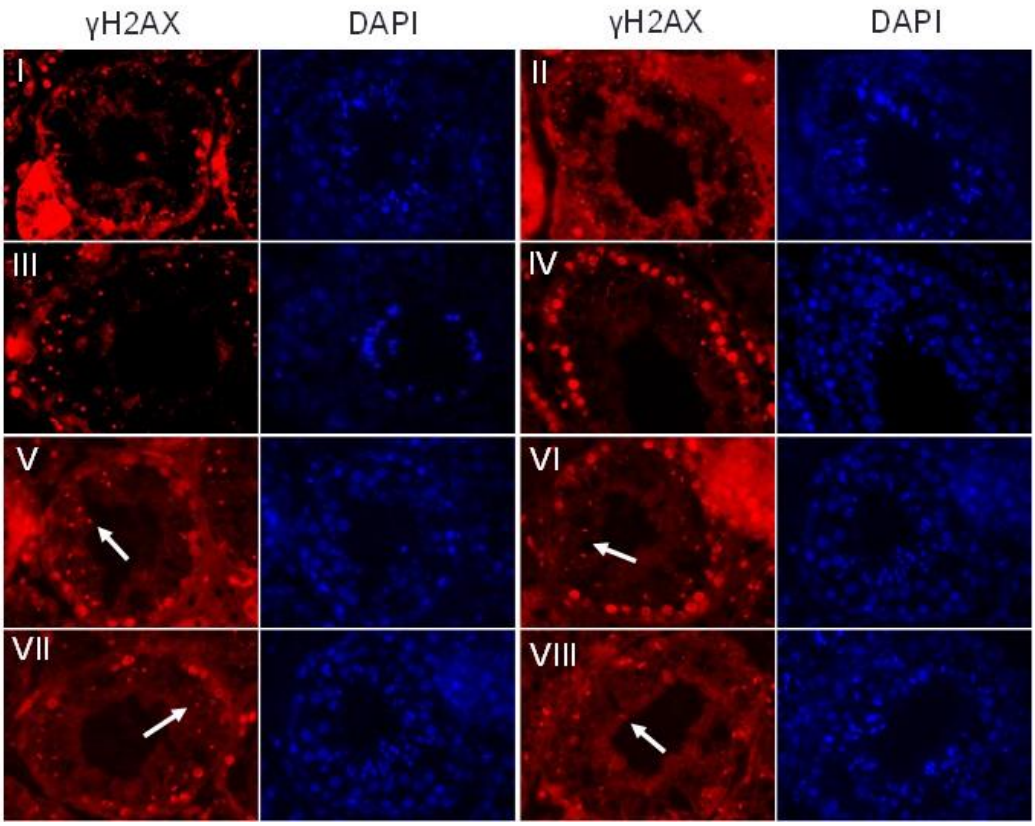

Figure 12. Immunofluorescence of γH2AX. Antibodies specific to phosphorylated H2AX confirm localization of the modified protein similar to the mouse in XY-bodies of spermatocytes (stages V, VI, arrow), leptotene, zygotene and early pachytene spermatocytes (stages V-VIII, I), and elongating spermatids (stages VI-VIII, I, arrows).

Gamma H2AX was not found in immature or mature testes, if present it would have been detected at approximately 16 kDa. H2AZ was detected in both the immature and mature testes at approximately 14 kDa.

Transition Protein 1 and Protamine 1

Expression patterns of transition protein 1 and protamine 1 were assessed to examine stallion nucleoprotein exchange using immunofluorescence and western blot analysis. The appearance of TP1 marks the beginning of the nucleoprotein exchange in elongating spermatids. As shown in Figure 14, transition protein 1 is present in round

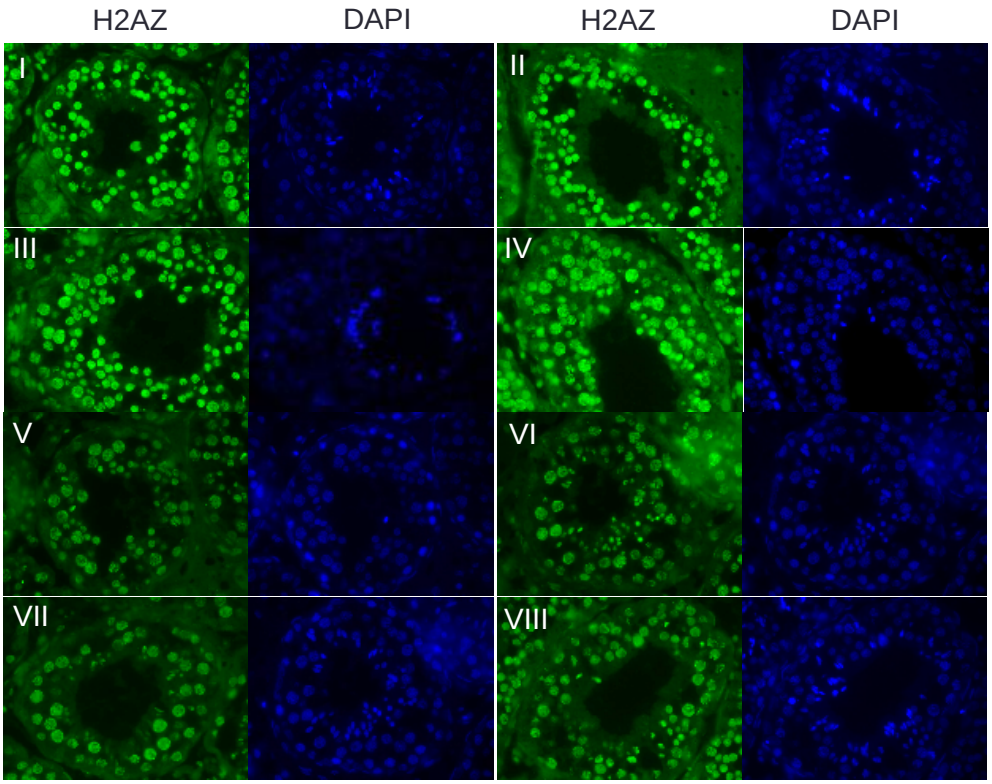

Figure 13. Immunofluorescence of H2AZ. H2AZ was expressed in pachytene spermatocytes and began to become undetectable as elongating spermatid chromatin condensed (stages VIII-II, Sd8 –Sd10).

spermatids during stage 5 and in elongating spermatids during stages 6 through 1. Throughout its presence in elongating spermatids, the expression intensity decreases, with just a small amount present in stage 2. During stage 3 after complete transition protein removal, a haze could be observed around the lumen. As shown in Figure 15, protamine 1 is present in elongating spermatids during stages 8 through 4.

Western blot analysis was completed on immature and mature testes for transition protein 1 (Figure 16). Transition protein 1 was detected in mature testes at approximately 10 kDa. There was no transition protein 1 detected in immature testes.

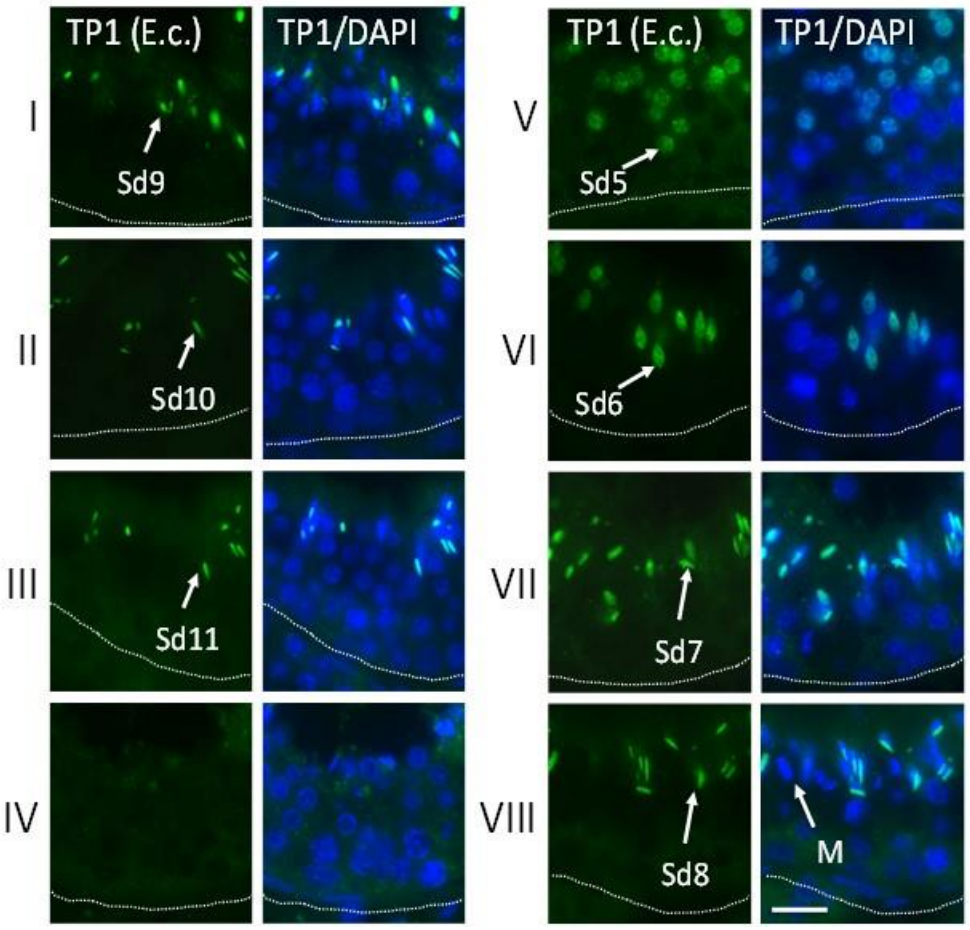

Figure 14. Immunofluorescence of transition protein 1. Transition protein 1 (TP1) began to be inserted into nuclear chromatin in Sd5 spermatids (stage V) of the stallion and was never detectable in nuclei of cell types other than elongating spermatids. The dotted white lines indicate the position of the tubular basal membrane for orientation. Scale bar, 20μm. (Ketchum et al., 2018)

Stallion Sperm

Semen samples were collected for artificial insemination purposes from Select Breeders Services in Maryland and one of their affiliates Four Sixes Ranch in Texas. Thirty-two stallion semen samples were donated to our lab with no history or fertility data included, creating a blind study.

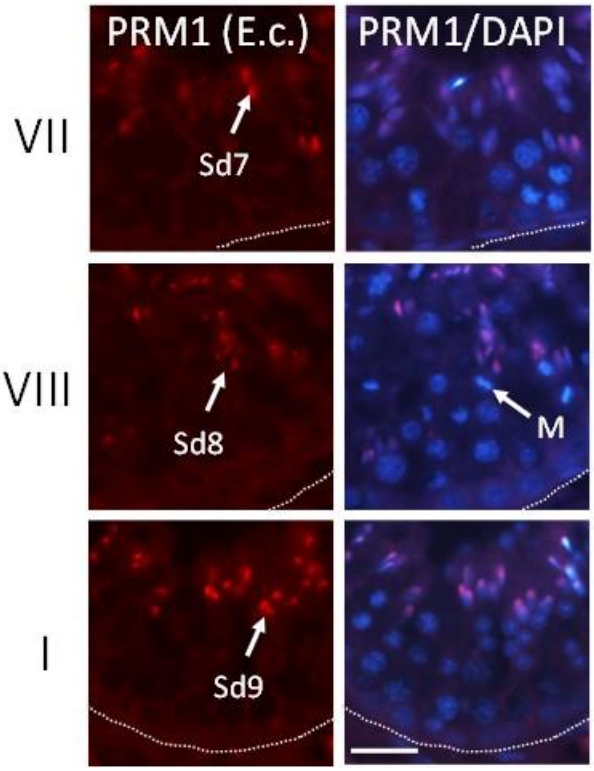

Figure 15. Immunofluorescence of protamine 1. Protamine 1 (PRM1) appeared in elongating spermatids, beginning in Sd7 spermatids and persisted afterwards (stage VII) until spermiation, as expected. (Ketchum et al., 2018)

Stallion sperm samples were evaluated using two different experimental procedures: western blot analysis and CMA3 staining. The western blot model, examined the amount of testis specific histone H2B (TH2B) in an allotment of sperm from each stallion. This model provided us a statistical amount of TH2B present, less TH2B indicating good fertility and more TH2B indicating bad fertility. The CMA3 model, detected packaging errors based upon protamine deficiency in individual sperm. This model provided us a percentage of the sperm that were not packaged correctly. These two models examine differing factors associated to fertility and thus gave differing results when predicting each stallion's fertility.

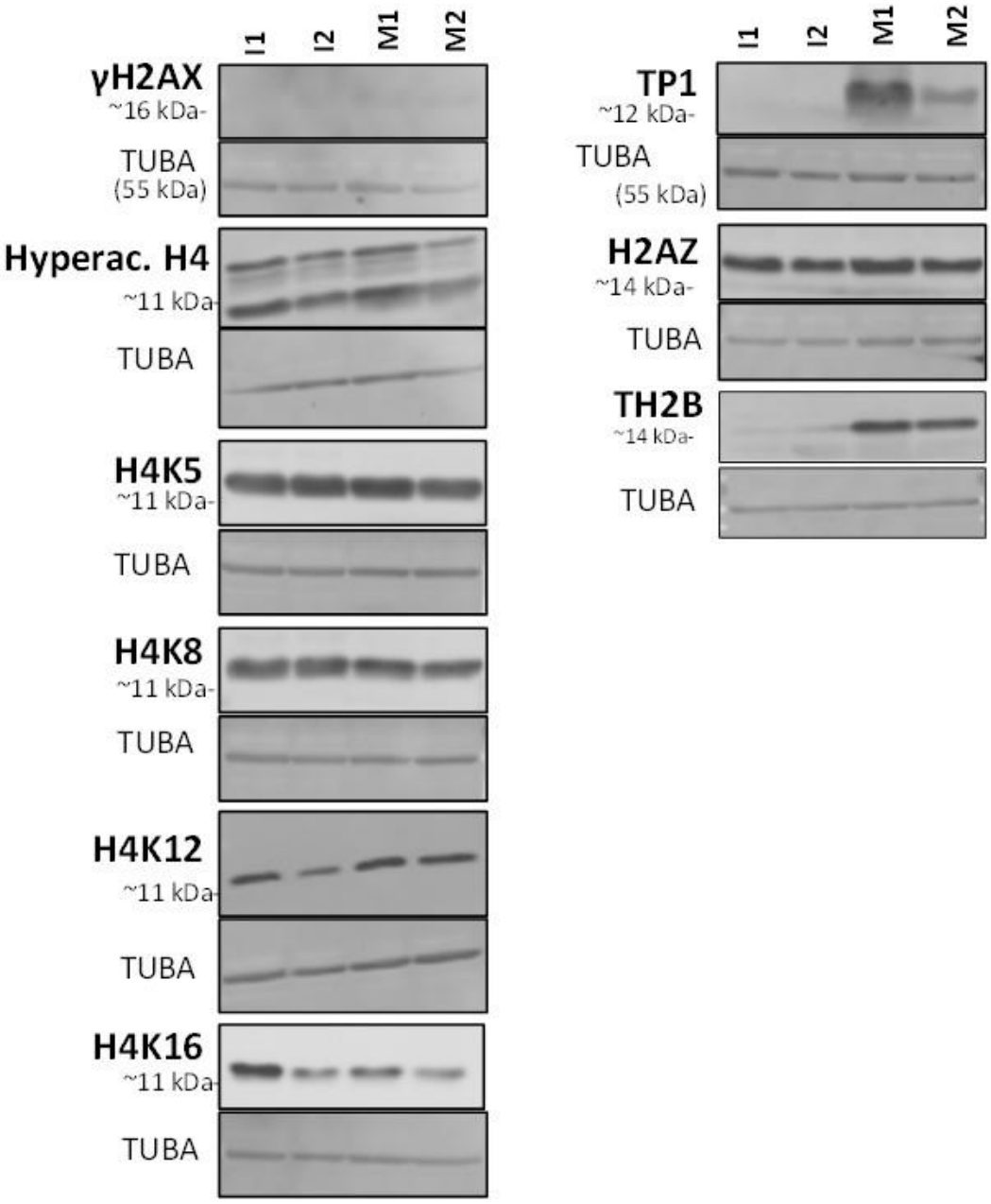

Figure 16. Western blot results using antibodies against candidate proteins. I1, I2: Immature horse testis lysates (two different animals) with incomplete spermatogenesis, M1, M2: Mature horse testes with full spermatogenesis (2 different animals). TUBA: alpha tubulin (marker protein used as quantitative loading control)

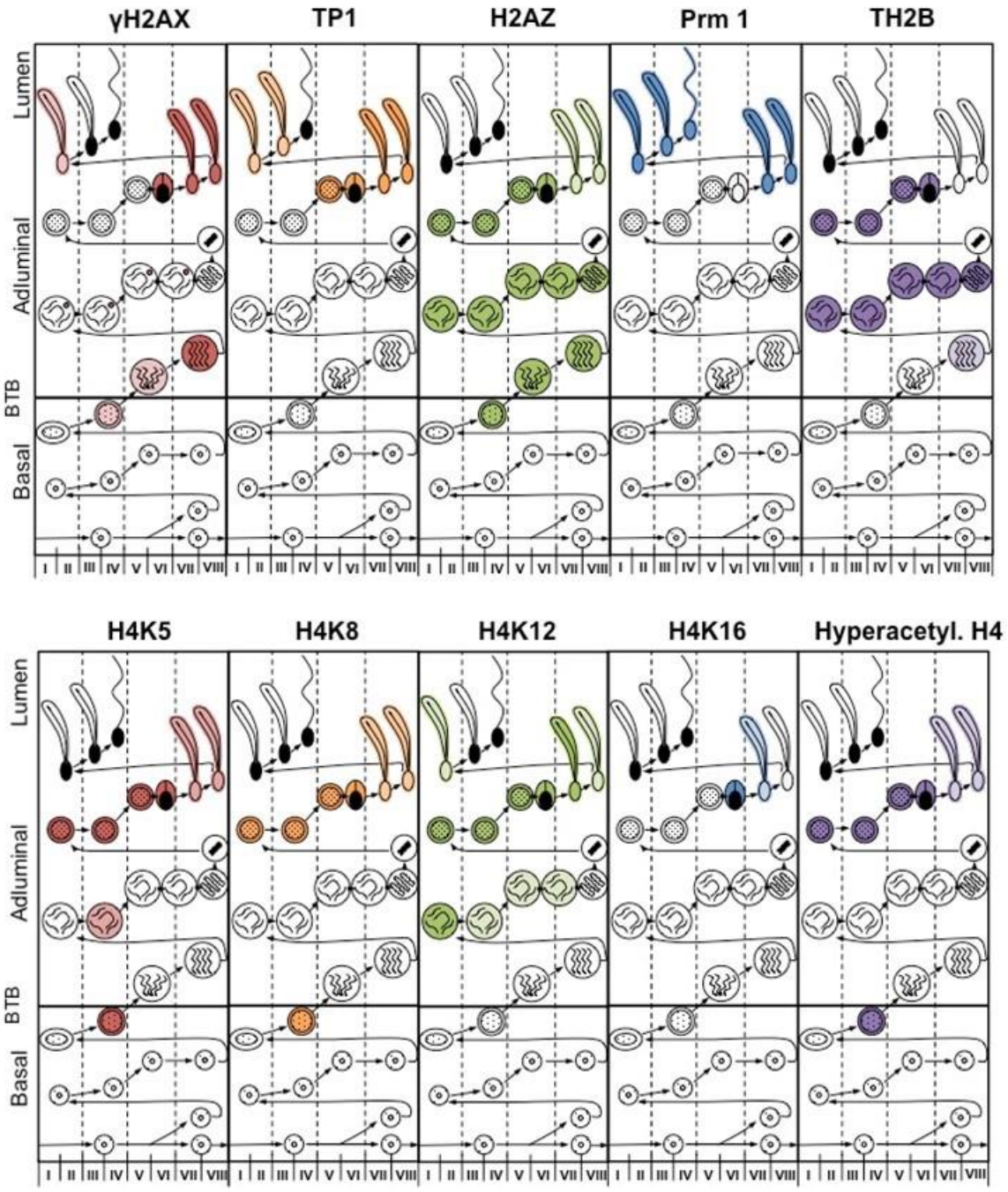

Figure 17. Overview scheme summarizing the results of the immunofluorescence analyses. Each column shows a specific protein expression. Thin columns divided by dotted lines separate each stage indicated at the bottom of each column. The progression from A-spermatogonia to elongated spermatids is shown using arrows. The left margin of the figure shows where in the tubule these cell types are found, starting at the basal membrane, blood testis barrier (BTB), adluminal, and the cells found directly next to the lumen.

Western Blot analyses

Raw semen samples from 32 stallions were assessed for TH2B levels using western blot analyses (Figure 18). Alpha-tubulin was used as a loading control. ImageJ computer analysis was used to calculate the TH2B intensity of each band (Table 3). Stallions with higher TH2B levels are predicted to have poorer fertility results than those stallions with lower TH2B levels.

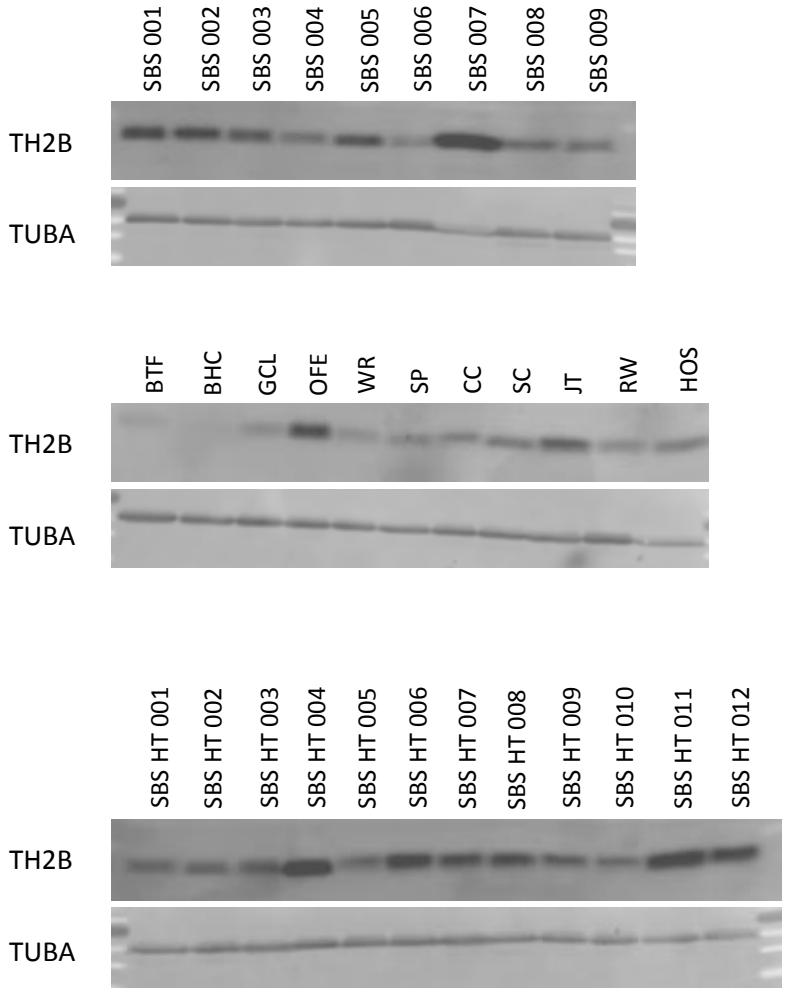

Figure 18. TH2B western blot results from 32 stallions' raw semen samples donated by Select Breeders Service (Chesapeake City, MD). Alpha-tubulin (TUBA) was used as a loading control and is found at 55 kDa. TH2B is located at 14 kDa.

Table 3

TH2B Levels Formulated from the Intensity of the Western Blot Bands for Each Stallion Using ImageJ Computer Analysis

Horse ID	TH2B level
SBS HT-001	2621.0
SBS HT-002	3069.0
SBS HT-003	3283.8
SBS HT-004	7184.4
SBS HT-005	3648.3
SBS HT-006	6902.2
SBS HT-007	5174.9
SBS HT-008	5343.6
SBS HT-009	3510.5
SBS HT-010	2944.5
SBS HT-011	8571.0
SBS HT-012	7180.7
SBS-001	4912.3
SBS-002	4973.7
SBS-003	3817.4
SBS-004	2387.5
SBS-005	4464.3
SBS-006	2024.6
SBS-007	8312.0
SBS-008	3055.2
SBS-009	2418.5
BTF	987.8
BHC	551.7
GCL	2404.9
OFE	6903.0
WR	1971.8
SP	1692.0
CC	2699.8
SC	3629.5
JT	6183.9
RW	2718.6
HOS	3640.2

Note. Stallions with higher TH2B levels are predicted to have poorer fertility results then those stallions with lower TH2B levels.

CMA3 Assays

Sperm smear slides were prepared using the 32 stallion semen samples donated by Select Breeders Services. Positive and negative control mouse sperm smear slides were used in addition to the stallion sperm smear slides to ensure the procedure worked (Figure 19). Two CMA3 experiments were completed to increase statistical accuracy. Higher staining intensity of CMA3 indicates that a particular sperm cell is not packaged properly.

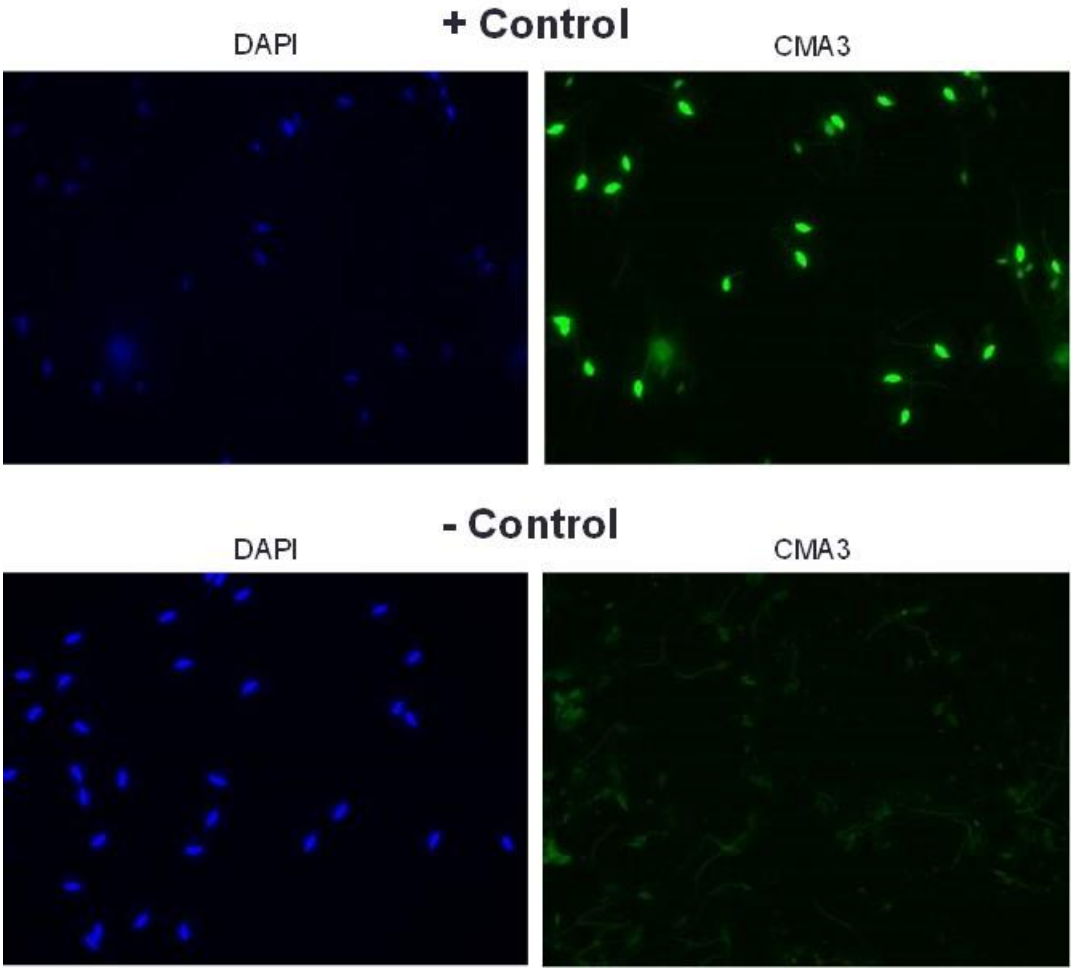

Figure 19. CMA3 positive and negative control slides were used to verify that the experiment worked properly. Sperm from a transgenic Parg$^{-/-}$ mouse (Meyer lab) was used as a positive control (green fluorescence of the chromomycin A3 dye intercalated into the DNA), while a wild-type mouse was used as a negative control.

Four parameters were examined for each of the two CMA3 experiments. The mean density (intensity) of each sperm cell that was imaged was used to calculate each of the four parameters. The first parameter, the percentage of outliers away from one standard deviation of the mean, was used to find what percentage of each stallion's sperm sample was CMA3 positive within one standard deviation from the mean (Table 4). The second parameter, the percentage of outliers away from two standard deviations from the mean, was used to find a more conservative percentage of each stallion's sperm sample was CMA3 positive. The third and forth parameters, mean and median, were used to assess if the mean and median of the overall sperm intensity levels skewed to the positive or negative side of the spectrum (Table 4). Fertility rankings based on these four parameters differs slightly between experiments and between parameters.

Stallion Breeding Data

Actual breeding data from Select Breeders Services on the breeding performance of the stallions were obtained after the conclusion of the analyses performed at USU (Table 5). If correlations between the predictive results of these analyses and the actual field data exist, they are likely weak and require more in-depth statistical analyses. It is likely that the inclusion of additional parameters, such as testes circumference and motile sperm concentration, are needed to make a more accurate prediction of stallion fertility.

Table 4

CMA3 Results

Horse ID	1st CMA3: 1SD % Outliers	2nd CMA3: 1SD % Outliers	Combined: 1SD % Outliers	1st CMA3: 2SD % Outliers	2nd CMA3: 2SD % Outliers	Combined: 2SD % Outliers	1st CMA3: Mean	2nd CMA3: Mean	Combined: Mean	1st CMA3: Median	2nd CMA3: Median	Combined: Median
SBS HT-001	2.75	4.88	3.815	1.57	3.90	2.74	8.69	12.79	10.74	8.18	10.84	9.51
SBS HT-002	6.77	6.95	6.86	4.09	4.17	4.13	13.60	20.28	16.94	11.17	17.29	14.23
SBS HT-003	8.60	4.03	6.315	1.79	2.49	2.14	9.90	16.00	12.95	9.48	14.66	12.07
SBS HT-004	4.41	6.70	5.555	2.41	3.25	2.83	11.64	24.34	17.99	11.19	23.28	17.24
SBS HT-005	7.56	11.44	9.50	4.74	7.00	5.87	16.70	30.29	23.50	13.51	25.59	19.55
SBS HT-006	5.72	8.02	6.87	4.32	4.77	4.55	11.36	24.82	18.09	9.15	21.79	15.47
SBS HT-007	5.56	4.98	5.27	2.40	2.33	2.37	13.25	17.51	15.38	12.66	17.09	14.88
SBS HT-008	8.93	12.79	10.86	2.74	3.52	3.13	15.58	18.03	16.81	14.34	16.58	15.46
SBS HT-010	15.00	15.05	15.025	4.09	3.00	3.55	11.37	26.12	18.75	10.88	25.37	18.13
SBS HT-011	4.33	5.96	5.145	2.07	3.26	2.67	9.24	22.01	15.63	8.88	20.92	14.90
SBS HT-012	4.54	13.31	8.925	2.55	5.47	4.01	11.93	26.49	19.21	10.44	23.59	17.02
SBS-001	5.48	8.21	6.845	2.53	1.93	2.23	18.95	17.06	18.01	18.00	16.56	17.28
SBS-002	2.68	7.61	5.145	1.39	2.01	1.70	11.22	18.93	15.08	10.62	18.42	14.52
SBS-003	4.42	8.14	6.28	2.34	3.82	3.08	14.44	22.33	18.39	13.52	21.45	17.49
SBS-004	5.40	7.92	6.66	2.79	3.42	3.11	16.13	22.33	19.23	14.50	21.50	18.00
SBS-005	5.15	4.70	4.925	2.72	2.25	2.49	12.00	14.33	13.17	11.25	13.76	12.51
SBS-006	3.01	3.98	3.495	1.92	1.84	1.88	11.79	18.80	15.30	11.23	18.07	14.65

(*table continues*)

Horse ID	1st CMA3: 1SD % Outliers	2nd CMA3: 1SD % Outliers	Combined: 1SD % Outliers	1st CMA3: 2SD % Outliers	2nd CMA3: 2SD % Outliers	Combined: 2SD % Outliers	1st CMA3: Mean	2nd CMA3: Mean	Combined: Mean	1st CMA3: Median	2nd CMA3: Median	Combined: Median
SBS-007	7.58	5.92	6.75	3.79	3.01	3.40	13.17	16.33	14.75	10.94	15.39	13.17
SBS-008	6.76	5.72	6.24	4.94	3.88	4.41	16.00	23.25	19.63	12.98	21.78	17.38
SBS-009	3.58	4.44	4.01	2.78	2.47	2.63	14.62	15.48	15.05	13.42	14.01	13.72
BTF	1.20	5.19	3.20	0.52	1.21	0.87	8.24	21.57	14.91	7.69	21.52	14.61
BHC	1.57	4.23	2.90	0.90	1.63	1.27	8.12	21.55	14.84	7.85	21.05	14.45
OFE	4.65	5.81	5.23	2.88	3.93	3.41	9.11	20.81	14.96	7.88	18.85	13.37
WR	2.03	3.59	2.81	1.55	1.64	1.60	8.25	16.39	12.32	7.39	15.93	11.66
SP	1.73	3.15	2.44	0.99	1.64	1.32	7.24	14.54	10.89	6.94	13.78	10.36
CC	3.07	3.85	3.46	1.62	2.07	1.85	9.99	21.52	15.76	9.56	20.93	15.25
SC	4.82	7.20	6.01	3.11	4.83	3.97	8.69	20.70	14.70	7.06	18.37	12.72
JT	3.19	4.79	3.99	1.39	2.40	1.90	7.67	20.37	14.02	7.36	20.08	13.72
RW	3.12	4.39	3.76	2.63	2.62	2.63	7.85	18.22	13.04	6.67	16.93	11.80
HOS	3.57	5.70	4.64	2.74	2.53	2.64	6.37	21.44	13.91	5.51	20.59	13.05

Note. Two CMA3 experiments were completed on 32 stallion sperm smears. This figure shows the four parameters that were examined broken down for each of the two experiments and an average of both experiments. The mean density (intensity) of each sperm cell that was imaged was used to calculate each of the 4 parameters. The first parameter, the percentage of outliers away from one standard deviation of the mean, was used to find what percentage of each stallion's sperm sample was CMA3 positive within one standard deviation from the mean. The second parameter, the percentage of outliers away from two standard deviations from the mean, was used to find a more conservative percentage of each stallion's sperm sample was CMA3 positive. The third and forth parameters, mean and median, were used to assess if the mean and median of the overall sperm intensity levels skewed to the positive or negative side of the spectrum.

Table 5

Breeding Data from Select Breeders Services

Horse ID	Total # of mares bred	First cycle conception rate (%)	End of season pregnancy rate (%)
SBS HT-001	8	63	63
SBS HT-002	13	69	85
SBS HT-003	36	58	72
SBS HT-004	28	70	78
SBS HT-005	39	70	74
SBS HT-006	14	57	79
SBS HT-007	9	70	90
SBS HT-008	10	40	50
SBS HT-010	21	52	71
SBS HT-011	10	40	60
SBS HT-012	30	60	80
SBS-001	11	27	82
SBS-002	21	52	81
SBS-003	18	56	72
SBS-004	8	38	38
SBS-005	4	25	25
SBS-006	17	65	76
SBS-007	3	67	100
SBS-008	2	0	50
SBS-009	30	40	73
BTF	22	55	77
BHC	281	48	75
OFE	124	55	78
WR	65	46	72
SP	50	66	88
CC	20	35	50
SC	7	71	71
JT	67	72	88
RW	74	45	77
HOS	71	45	65

CHAPTER V

DISCUSSION

This study presents the first comprehensive characterization of equine nucleoprotein exchange studying TH2B, γH2AX, H2AZ, TP1, Prm1, hyper-acetylated H4, H4K5ac, H4K8ac, H4K1ac, and H4K16ac in testis. We described the equine nucleoprotein exchange during spermatogenesis to identify candidate marker proteins of incomplete sperm chromatin maturation. When comparing the nucleoprotein exchange in horse to the foremost studied models, mouse and human, it is apparent that there are differences in the stallion that encourage rethinking of the current paradigms for how histones are exchanged for protamines during spermiogenesis. A review of the literature was conducted and the findings were published within the framework of the present project (Meyer et al., 2017).

The finding that in the stallion H4 acetylation in positions K5, K8 and K12 occurs immediately after meiosis was unexpected because in mice these events are prevalent only at the onset of spermatid nuclear elongation (Shirakata, Hiradate, Inoue, Sato, & Tanemura, 2014). Using the same experimental conditions and antibodies, we confirmed the puzzling difference in H4 lysine acetylation between the species by analyzing mouse and stallion tissue side by side (Figure 20). Most of the mouse data that I generated for this project are not shown in this thesis, but they are published (Ketchum et al., 2018). Several studies conducted in mice, rats and Drosophila reported highly acetylated H4 to be present in elongating spermatids and associated with histone displacement in (Dhar, Thota, & Rao, 2012; Goudarzi, Shiota, Rousseaux, & Khochbin,

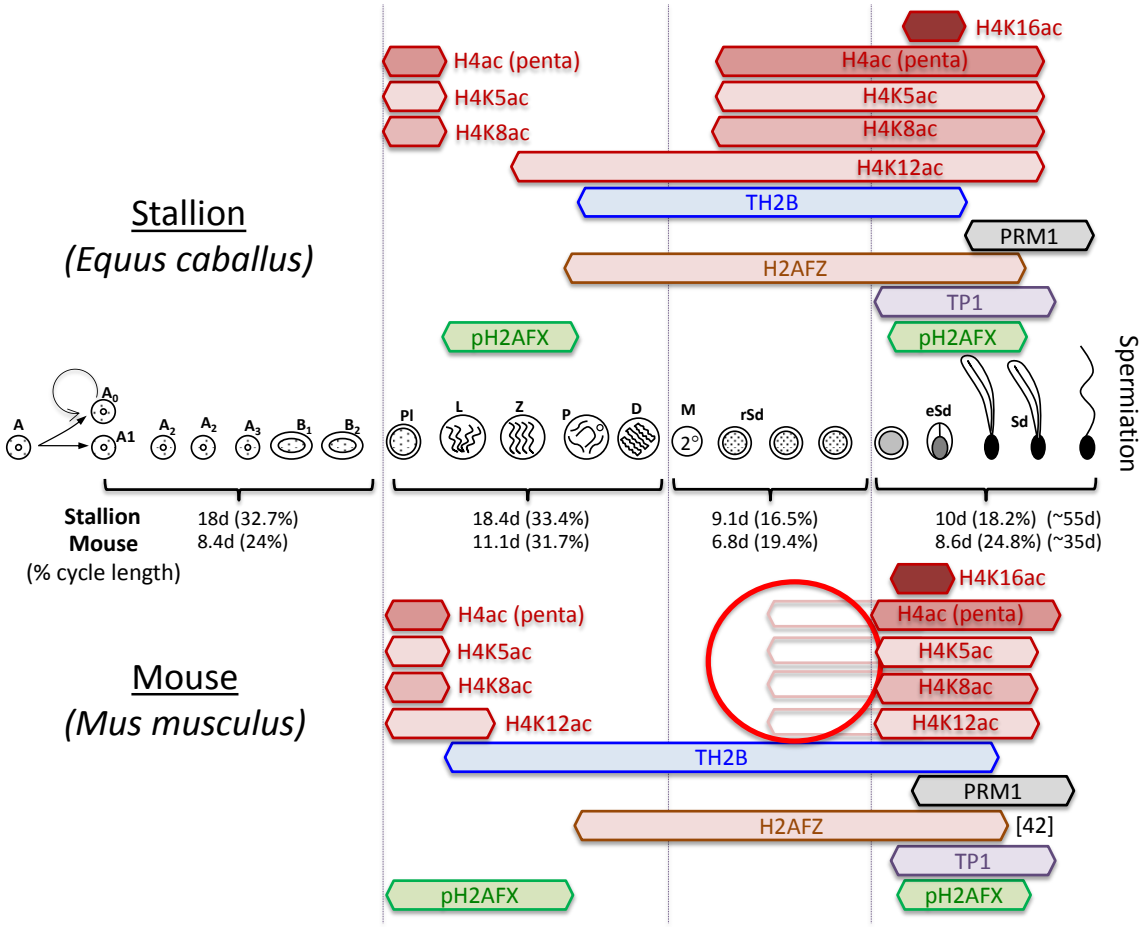

Figure 20. Summary image: Similarities and differences between equine and murine chromatin remodeling during spermatogenesis. When aligning cell types and timelines of equine (top) and murine (bottom) spermatogenesis in this overview over the data obtained in this study, time intervals between key events in spermatogenesis were calculated using known cycle length data and expressed as fractions of total cycle lengths (in %) in stallion and mouse. Comparing these intervals revealed that timing of events in spermatogenesis of the two animals is relatively similar. Developmental germ cell stages (using the stallion in the graphic), where the denoted proteins and posttranslational protein modifications were detectable, are indicated by the horizontal bars. The main difference between the two species was in the timing of H4 acetylation events which is highlighted by the red circle. The pale bars in the red circle indicate that some studies have previously shown the possibility of some weak H4 acetylation in spermatid steps Sd1-8 of the mouse. Mouse immunofluorescence data were obtained using the same antibodies that were used for the analyses of the stallion), except for H2AFZ. The H2AFZ antibody that was used in stallion testis sections did not recognize the mouse protein, and published data obtained with a custom antiserum in mice were used for the comparison (Ketchum et al., 2018).

2014; Hazzouri et al., 2000; Meistrich et al., 1992; Shirakata et al., 2014). A study in the human demonstrated H4 hyperacetylation during all developmental steps of round and elongated spermatids utilizing an antiserum raised against hyperacetylated (penta) H4 histones (Sonnack, Failing, Bergmann, & Steger, 2002). This is reminiscent of our data in the stallion, supporting the view that the timing of histone hyperacetylation may be a species-specific event. Progressive acetylation of H4 in lysine residues K5, K8, K12 and K16 adds a negative charge to the histone and thus, in addition to the acetylation of other critical lysine residues in other histones, such as H3K122 and H3K64, which destabilizes the nucleosome and weakens its binding to the DNA (Goudarzi et al., 2014). H4K5ac and H4K8ac are collectively bound by the first bromodomain (BD1) of BRDT (Miller et al., 2016; Morinière et al., 2009; Pivot-Pajot et al., 2003). Binding of BRDT to acetylated H4 is essential for successful histone removal and sperm development because deletion of BD1 results in deformed sperm with excessive histone retention, teratozoospermia (sperm with abnormal morphology) and male infertility (Shang, Nickerson, Wen, Wang, & Wolgemuth, 2007). The precise function of BRDT in histone eviction from spermatid chromatin is not well understood and different models have been proposed such as direct mechanical ‘squeezing’ of chromatin fibers by polymerizing BRDT proteins (Gaucher et al., 2012). This process likely involves binding of other proteins including beta actin and SMARCE1 (Dhar et al., 2012). SMARCE1 is a subunit of the SWI/SNF family of ATP-dependent chromatin remodelers and its recruitment by BRDT in the presence of hyperacetylated H4 provides a possible mechanism by which H4 hyperacetylation results in nucleosome removal (Dhar et al., 2012). The data presented here raises the question

whether BRDT binding to H4K5ac and H4K8ac, and possibly H4K12ac, is sufficient to recruit SMARCE1 and elicit nucleosome eviction, because if that was the case, the early arrival of these marks in round spermatids immediately after meiosis would likely result in nucleosome eviction in the resulting Sd1 spermatids. However, this does not seem to be the case as we find the deposition of TP1 to occur approximately 1 week after meiosis in elongating spermatids (Sd6 and Figure 14). Acetylation of H4K16 in elongating spermatids occurs across all species of mammals. Since all other pertinent H4 acetylation marks are present during early spermiogenesis, data suggests that H4K16 acetylation may be of importance to histone eviction. H4K16 acetylation may provide the last negative charge needed to tip the balance towards the binding of a remodeling complex via BRDT or another bromodomain protein. It is likely that other bromodomain proteins, such as BRD4 (Bryant et al., 2015) and other protein factors may also play a role in the removal of nucleosomes from spermatid chromatin, but details are not yet well understood.

H4K16 acetylation occurs independently from H4K5 and H4K8 acetylation (Sin et al., 2012) and is mediated by the acetyltransferase KAT8 (also known as MYST1, MOF). KAT8 is a necessary component of DNA strand break repair where it is phosphorylated by ATM in response to DNA double strand breaks. KAT8 colocalizes with phosphorylated H2AFX in the vicinity of DNA strand breaks in somatic cells (Gupta et al., 2014). Intriguingly, elongating spermatids undergo genome-wide DNA torsional relaxation during a short time window when topoisomerase II beta (TOP2B) activity introduces controlled DNA double-strand breaks in a decatenation reaction (Laberge & Boissonneault, 2005; Macron & Boissonneault, 2004; Smith & Haaf, 1998).

TOP2B-mediated DNA decatenation activates DNA strand break-dependent DNA damage signaling pathways mediated by the ATM- and poly(ADP-ribose) polymerase-(PARP) pathways in mouse elongating spermatids (Meyer-Ficca et al., 2005, Meyer-Ficca, Ihara, et al., 2011). PARP activity negatively regulates the activities of TOP2B (Meyer-Ficca, Lonchar, et al., 2011) and ATM (Haince et al., 2007; Watanabe et al., 2004), supporting the importance of DNA damage response pathways in the chromatin remodeling process that takes place in elongating spermatids.

In conclusion, data obtained in the stallion show a temporal separation between acetylation of H4K5, H4K8 and H4K12 acetylation (H4 hyperacetylation) and the insertion of TP1 as an indicator of beginning histone eviction. The results support the hypothesis that H4K16ac is the key acetylation mark that initiates the nucleoprotein transition from the histone- to a protamine-based chromatin structure and therefore provides another link between histone eviction and DNA strand break repair pathways elicited by TOP2B activity in the elongating spermatid. The stallion may be a better-suited model, over the mouse, for the epigenetic regulation of chromatin regulation of chromatin remodeling events in human because of the strong acetylation of H4K5, H4K8 and H4K12 in all spermatids, while round and elongated spermatids are also observed in humans (Sonnack et al., 2002). We identified TH2B as a potential marker of poor sperm chromatin quality in the stallion but its predictive value could not be conclusively demonstrated. It is likely that additional parameters, such as testis circumference or the number and concentration of motile sperm in the fresh ejaculate, are needed to effectively predict stallion breeding performance.

REFERENCES

Ahmed, E. A., de Boer, P., Philippens, M. E. P., Kal, H. B., & de Rooij, D. G. (2010). Parp1-XRCC1 and the repair of DNA double strand breaks in mouse round spermatids. *Mutation Research, 683*(1-2), 84-90.

Amann, R. P. (1981a). A review of anatomy and physiology of the stallion. *Equine Veterinary Science, May/June*, 83-105.

Amann, R. P. (1981b). Spermatogenesis in the stallion: a review. *Equine Veterinary Science, July/August,* 131-139.

Arpanahi, A., Brinkworth, M., Iles, D., Krawetz, S. A., Paradowska, A., Platts, A. E., … Miller, D. (2009). Endonuclease-sensitive regions of human spermatozoal chromatin are highly enriched in promoter and CTCF binding sequences. *Genome Research. 19*(8), 1338-1349.

Bao, J., & Bedford, M. T. (2016). Epigenetic regulation of the histone-to-protamine transtition during spermiogenesis. *Reproduction, 151*(5), 55-R70.

Braun, R. E. (2001). Packaging paternal chromosomes with protamine. *Nature Genetics. 28*(1), 10-12.

Brito, L. (2007). Evaluation of stallion sperm morphology. *Clinical Techniques Equine Practice. 6*, 249-264.

Bryant, J. M., Donahue, G., Wang, X., Meyer-Ficca, M., Luense, L. J., Weller, A. H., … Berger, S. L. (2015). Characterization of BRD4 during mammalian postmeiotic sperm development. *Molecular Cell Biology. 35*(8), 1433-1448.

Brykczynska, U., Hisano, M., Erkek, S., Ramos, L., Oakeley, E. J., Roloff, T. C., … Peters, A. H. (2010). Repressive and active histone methylation mark distinct promoters in human and mouse spermatozoa. *Nature Structural & Molecular Biology. 17*(6), 679-687.

Carone, B. R., Hung, J. H., Hainer, S. J., Chou, M. T., Carone, D. M., Weng, Z., … Rando, O. J. (2014). High-resolution mapping of chromatin packaging in mouse embryonic stem cells and sperm. *Developmental Cell. 30*(1), 11-22.

Casey, P. J., Gravance, C. G., Davis, R. O., Chabot, D. D., & Liu, I. K. (1997). Morphmetric differences in sperm head dimensions of fertile and subfertile stallions. *Theriogenology, 47,* 575-582.

Cavalcanti, M. C. O., Rizgalla, M., Geyer, J., Failing, K., Litzke, L. F., & Bergmann, M. (2009). Expression of histone 1 (H1) and testis-specific histone 1 (H1t) genes during stallion spermatogenesis. *Animal Reproduction Science, 111,* 220-234.

Celeste, A., Peterson, S., Romanienko, P. J., Fernandez-Capetillo, O., Chen, H. T., Sedelnikova, O. A., … Nussenzweig, A. (2002). Genomic instability in mice lacking histon H2AX. *Science, 296,* 922-927.

Cho, C., Willis, W. D., Goulding, E. H., Jung-Ha, H., Choi, Y. C., Hecht, N. B., & Eddy, E. M. (2001). Haploinsufficiency of protamine-1 or −2 causes infertility in mice. *Nature Genetics., 28,* 82-86.

Clermont, Y. (1963). The cycle of the seminiferous epithelium in man. *American Journal of Anatomy, 112,* 35-51.

Clermont, Y. (1966). Renewal of spermatogonia in man. *American Journal of Anatomy, 118*(2), 509-524.

Clermont, Y. (1972). Kinetics of spermatogenesis in mammals: seminiferous epithelium cycle and spermatogonial renewal. *Physiological Reviews., 52,* 198-236.

Costa, G. M. J., Avelar, G. F., Rezende-Neto, J. V., Campos-Junior, P. H. A., Lacerda, S. M. S. N., Andrade, B. S. C., … Franca, L. R. (2012). Spermatogonial stem cell markers and niche in equids. *PLOS ONE, 7*(8), 1-13.

de Oliveira, R. V., Dogan, S., Belser, L. E., Kaya, A., Topper, E., Moura, A., … Memili, E. (2013). Molecular morphology and function of bull spermatozoa linked to histones and associated with fertility. *Reproduction, 146*(3), 263-272.

Dhar, S., Thota, A., & Rao, M. R. S. (2012). Insights into role of bromodomain, testis-specific (Brdt) in acetylated histone H4-dependent chromatin remodeling in mammalian spermiogenesis. *The Journal of Biological Chemistry, 287,* 6387-6405.

Erkek, S., Hisano, M., Liang, C. Y., Gill, M., Murr, R., Dieker, J., & Peters, A. H. (2013). Molecular determinants of nucleosome retention at CpG-rich sequences in mouse spermatozoa. *Nature Structural Molecular Biology. 20*(7), 868-875.

Faast, R., Thonglairoam, V., Schulz, T. C., Beall, J., Wells, J. R., Taylor, H., … Lyons, I. (2001). Histone variant H2A.Z is required for early mammalian development. *Current Biology, 11,* 1183-1187.

Gaucher, J., Boussouar, F., Montellier, E., Curtet, S., Buchou, T., Bertrand, S., … Khochbin, S. (2012). Bromodomain-dependent stage-specific male genome programming by Brdt. *The EMBO Journal. 31,* 3809-3820.

Goudarzi, A., Shiota, H., Rousseaux, S., & Khochbin, S. (2014). Genome-scale acetylation-dependent histone eviction during spermatogenesis. *Journal of Molecular Biology, 426,* 3342-3349.

Govin, J., Caron, C., Lestrat, C., Rousseaux, S., & Khochbin, S. (2004). The role of histones in chromatin remodeling during mammalian spermiogenesis. *European Journal of Biochemistry, 271,* 3459-3469.

Grimes, S. R., Meistrich, M. L., Platz, R. D., & Hnilica, L.S. (1997). Nuclear protein transitions in rat testis spermatids. *Experimental Cell Research. 110*(1), 31-39.

Gupta, A., Hunt, C. R., Hegde, M. L., Chakraborty, S., Chakraborty, S., Udayakumar, D., … Pandita, T. K. (2014). MOF phosphorylation by ATM regulates 53BP1-mediated double-strand break repair pathway choice. *Cell Reports, 8*(1). 177-189.

Haince, J. F., Kozlov, S., Dawson, V. L., Dawson, T. M., Hendzel, M. J., Lavin, M. F., & Poirier, G. G. (2007). Ataxia telangiectasia mutated (ATM) signaling network is modulated by a novel poly(ADP-ribose)-dependent pathway in the early response to DNA-damaging agents. *The Journal of Biological Chemistry, 282,* 16441-16453.

Hamer, G., Roepers-Gajadien, H. L., van Duyn-Goedhart, A., Gademan, I. S., Kal, H. B., van Buul, P. P., & de Rooij, D. G. (2003). DNA double-strand breaks and gamma-H2AX signaling in the testis. *Biology of Reproduction, 68*(2), 628-634.

Hammoud, S. S., Nix, D. A., Hammoud, A. O., Gibson, M., Cairns, B. R., & Carrell, D. T. (2011). Genome-wide analysis identifies changes in histone retention and epigenetic modifications at developmental and imprinted gene loci in the sperm of infertile men. Human *Reproduction Oxford England, 26,* 2558-2569.

Hazzouri, M., Pivot-Pajot, C., Faure, A. K., Usson, Y., Pelletier, R., Sèle, B., Khochbin, S., & Rousseaux, S. (2000). Regulated hyperacetylation of core histones during mouse spermatogenesis: involvement of histone deacetylases. *European Journal of Cell Biology, 79,* 950-960.

Hess, R. A., & Renato de France, L. (2008). Spermatogenesis and cycle of the seminiferous epithelium. *Advances in Experimental Medicine and Biology, 636,* 1-15.

Ihara, M., Meyer-Ficca, M. L., Leu, N. A., Rao, S., Li, F., Gregory, B. D., … Meyer, R. G. (2014). Paternal poly (ADP-ribose) metabolism modulates retention of inheritable sperm histones and early embryonic gene expression. *PLoS Genetics. 10*(5), e1004317.

Johnson, L., Hardy, V. B., & Martin, M. T. (1990). Staging equine seminiferous tubules by nomarski optics in unstained histologic sections and in tubules mounted in toto to reveal the spermatogenic wave. *The Anatomical Record, 227,* 167-174.

Ketchum, C., Larson, C., McNeil, A., Meyer-Ficca, M. L., & Meyer, R. G. (2018). Histone H4 acetylation and chromatin remodeling events in equine spermatogenesis. *Bioogy of Reproduction, 98*(1), 115-129.

Kimmins, S., & Sassone-Corsi, P. (2005). Chromatin remodelling and epigenetic features of germ cells. *Nature, 434,* 583-589.

Kornberg, R. D. (1974). Chromatin structure: a repeating unit of histones and DNA. *Science, 184,* 868-871.

Laberge, R. M., & Boissonneault, G. (2005). On the nature and origin of DNA strand breaks in elongating spermatids. *Biology of Reproduction, 73*(2), 289-296.

Leduc, F., Maquennehan, V., Nkoma, G. B., & Boissonneault, G. (2008). DNA damage response during chromatin remodeling in elongating spermatids of mice. *Biology of Reproduction, 78,* 324-332.

Marcon, L., Boissonneault, G. (2004). Transient DNA strand breaks during mouse and human spermiogenesis new insights in stage specificity and link to chromatin remodeling. *Biology of Reproduction, 70,* 910-918.

Maze, I., Noh, K., Soshnev, A. A., & Allis, C. D. (2014). Every amino acid matters: essential contributions of histone variants to mammalian development and disease. *Nature Reviews. Genetics, 15,* 259-271.

McPherson, S. M., & Longo, F. J. (1992). Localization of DNase I-hypersensitive regions during rat spermatogenesis: Stage-dependent patterns and unique sensitivity of elongating spermatids. *Molecular Reproduction and Development, 31,* 268-279.

McPherson, S. M., & Longo, F. J. (1993). Nicking of rat spermatid and spermatozoa DNA: possible involvement of DNA topoisomerase II. *Developmental Biology, 158*(1), 122-130.

Meistrich, M. L., Trostle-Weige, P. K., Lin, R., Bhatnagar, Y. M., & Allis, C. D. (1992). Highly acetylated H4 is associated with histone displacement in rat spermatids. *Molecular Reproduction and Development, 31*(3), 170-181.

Meyer, R. G., Ketchum, C. C., & Meyer-Ficca, M. L. (2017). Heritable sperm chromatin epigenetics: a break to remember. *Biology of Reproduction, 97,* 784-797.

Meyer-Ficca, M. L., Ihara, M., Lonchar, J. D., Meistrich, M. L., Austin, C. A., Min, W., … Meyer, R. G. (2011). Poly(ADP-ribose) metabolism is essential for proper nucleoprotein exchange during mouse spermiogenesis. *Biology of Reproduction, 84*(2), 218-228.

Meyer-Ficca, M. L., Lonchar, J. D., Ihara, M., Meistrich, M. L., Austin, C. A., & Meyer, R.G. (2011). Poly(ADP-ribose) polymerases PARP1 and PARP2 modulate topoisomerase II beta (TOP2B) function during chromatin condensation in mouse spermiogenesis. *Biology of Reproduction, 84,* 900-909.

Meyer-Ficca, M. L., Scherthan, H., Burkle, A., & Meyer, R.G. (2005). Poly(ADP-ribosyl)ation during chromatin remodeling steps in rat spermiogenesis. *Chromosoma., 114*(1), 67-74.

Miller, T. C., Simon, B., Rybin, V., Grötsch, H., Curtet, S., Khochbin, S., … Müller, C. W. (2016). A bromodomain-DNA interaction facilitates acetylation-dependent bivalent nucleosome recognition by the BET protein BRDT. *Nature Communications, 7,* article number 13855.

Montellier, E., Boussouar, F., Rousseaux, S., Zhang, K., Buchou, T., Fenaille, F., … Khochbin, S. (2013). Chromatin-to-nucleoprotamine transition is controlled by the histone H2B variant TH2B. *Genes & Development, 27,* 1680-1692.

Morinière, J., Rousseaux, S., Steuerwald, U., Soler-López, M., Curtet, S., Vitte, A. L., … Petosa, C. (2009). Cooperative binding of two acetylation marks on a histone tail by a single bromodomain. *Nature, 461,* 664-668.

Morse-Gaudio, M., & Risley, M. S. (1994). Topoisomerase II expression and VM-26 induction of DNA breaks during spermatogenesis in Xenopus laevis. *Journal of Cell Science, 107,* 2887-2898.

Pesch S., & Bergmann M. (2006). Structure of mammalian spermatozoa in respect to viability, fertility and cryopreservation. *Micron, 37,* 597-612.

Pivot-Pajot, C., Caron, C., Govin, J., Vion, A., Rousseaux, S., & Khochbin, S. (2003). Acetylation-dependent chromatin reorganization by BRDT, a testis-specific bromodomain-containing protein. *Molecular and Cellular Biology., 23,* 5354-5365.

Rathke, C., Baarends, W. M., Awe, S., & Renkawitz-Pohl, R. (2014). Chromatin dynamics during spermiogenesis. *Biochimica et Biophysica Acta., 1839*(3), 155-168.

Reece, W. (2009). *Functional anatomy and physiology of domestic animals* (4th ed.). Ames, IA: Wiley-Blackwell

Risley, M. S., Einheber, S., & Bumcrot, D. A. (1986). Changes in DNA topology during spermatogenesis. *Chromosoma, 94*(3), 217-227.

Roca, J., & Mezquita, C. (1989). DNA topoisomerase II activity in nonreplicating, transcriptionally inactive, chicken late spermatids. *The EMBO Journal, 8,* 1855-1860.

Rousseaux, S., Faure, A. K., Caron, C., Lestrat, C., Govin, J., Hennebicq, S., … Khochbin, S. (2004). Organizing the sperm nucleus. *Gynecologie, Obstetrique & Fertilite, 32,* 785-791.

Schagdarsurengin, U., Paradowska, A., & Steger, K. (2012). Analyzing the sperm epigenome: Roles in early embryogenesis and assisted reproduction. *Nature Reviews. Urology, 9,* 609-619.

Shang, E., Nickerson, H. D., Wen, D., Wang, X., & Wolgemuth, D. J. (2007). The first bromodomain of Brdt, a testis-specific member of the BET sub-family of double-bromodomain-containing proteins, is essential for male germ cell differentiation. *Development Cambridge England, 134,* 3507-3515.

Shinagawa, T., Huynh, L. M., Takagi, T., Tsukamoto, D., Tomaru, C., Kwak, H., … Ishii, S. (2015). Disruption of Th2a and Th2b genes causes defects in spermatogenesis. *Development Cambridge England, 142,* 1287-1292.

Shirakata, Y., Hiradate, Y., Inoue, H., Sato, E., & Tanemura, K. (2014). Histone h4 modification during mouse spermatogenesis. *The Journal of Reproduction and Development, 60*(5), 383-387.

Sin, H. S., Barski, A., Zhang, F., Kartashov, A. V., Nussenzweig, A., Chen, J., … Namekawa, S. H. (2012). RNF8 regulates active epigenetic modifications and escape gene activation from inactive sex chromosomes in post-meiotic spermatids. *Genes & Development, 26,* 2737-2748.

Smith, A., & Haaf, T. (1998). DNA nicks and increased sensitivity of DNA to fluorescence in situ end labeling during functional spermiogenesis. *BioTechniques, 25*(3), 496-502.

Sonnack, V., Failing, K., Bergmann, M., & Steger, K. (2002). Expression of hyperacetylated histone H4 during normal and impaired human spermatogenesis. *Andrologia., 34*(6), 384-390.

Swierstra, E. E., Gebauer, M. R., & Pickett, B. W. (1974). Reproductive physiology of the stallion. *Journal of Reproduction and Fertility, 40,* 113-123.

"The Stallion: Breeding Soundness Examination & Reproductive Anatomy." (2007) University of Wisconsin-Madison. Archived from the original on 2007-07-16.

Watanabe, F., Fukazawa, H., Masutani, M., Suzuki, H., Teraoka, H., Mizutani, S., & Uehara, Y. (2004). Poly(ADP-ribose) polymerase-1 inhibits ATM kinase activity in DNA damage response. *Biochemical and Biophysical Research Communications, 319*(2), 596-602.

Wouters-Tyrou, D., Martinage, A., Chevaillier, P., & Sautiére, P. (1998). Nuclear basic proteins in spermiogenesis. *Biochimie, 80*(2), 117-128.

Zhang, K., Williams, K. E., Huang, L., Yau, P., Siino, J. S., Bradbury, E. M., … Burlingame, A. L. (2002). Histone acetylation and deacetylation. *Molecular & Cellular Proteomics, 1(7),* 500-508.

Zhao, M., Shirley, C. R., Hayashi, S., Marcon, L., Mohapatra, B., Suganuma, R., … Meistrich, M. L. (2004). Transition nuclear proteins are required for normal chromatin condensation and functional sperm development. *Genesis, 38*(4), 200-213.